Welcoming gallium- and indium-fumarate MOFs to the family

Zhang, Yue; Lucier, Bryan E. G.; Mckenzie, Sarah M.; Arhangelskis, Mihails; Morris, Andrew J.; Friščić, Tomislav; Reid, Joel W.; Terskikh, Victor V.; Chen, Mansheng; Huang, Yining

DOI:
10.1021/acsami.8b08562

Supporting Information

Welcoming Gallium- and Indium-fumarate MOFs to the Family: Synthesis, Comprehensive Characterization, Observation of Porous Hydrophobicity, and CO_2 Dynamics

Yue Zhang,[a] Bryan E. G. Lucier,[a] Sarah M. McKenzie,[a] Mihails Argangelskis,[b] Andrew J. Morris,[c] Tomislav Friščić,[b] Joel Reid,[d] Victor V. Terskikh,[e] Mansheng Chen,[a] Yining Huang[a,*]

[a] *Department of Chemistry, University of Western Ontario, London, Ontario, Canada N6A 5B7*

[b] *Department of Chemistry, McGill University, Montréal, Québec, Canada H3A 0G4*

[c] *School of Metallurgy and Materials, University of Birmingham, Edgbaston, Birmingham B15 2TT, UK*

[d] *Canadian Light Source, Saskatoon, Saskatchewan, Canada S7N 2V3*

[e] *Department of Chemistry, University of Ottawa, Ottawa, Ontario, Canada K1N 6N5*

**Corresponding author: yhuang@uwo.ca*

Table of contents

Experimental details for materials characterization S-3

Additional results and discussion S-13

Figure S1. Structure of MIL-53 S-21

Figure S2. pXRD patterns of Ga-fumarate synthesized under different conditions S-22

Figure S3. pXRD patterns of In-fumarate-E synthesized under different conditions S-23

Figure S4. pXRD patterns of In-fumarate-M synthesized under different conditions S-24

Figure S5. pXRD patterns of fumarate MOFs after exposure to various solvents S-25

Figure S6. TGA plots of various forms of Ga-fumarate S-26

Table S1. Experimental and calculated ^{69}Ga and ^{71}Ga NMR parameters of activated Ga-fumarate and Ga-fumarate-H_2O. S-27

Figure S7. TGA plots of various forms of In-fumarate-E S-28

Figure S8. ^{1}H MAS NMR spectra of various forms of Ga-fumarate S-29

Figure S9. ^{13}C CP/MAS NMR spectra of various forms of Ga-fumarate S-30

Figure S10. ^{1}H MAS NMR spectra of various forms of In-fumarate-E S-31

Figure S11. ^{13}C CP/MAS SSNMR spectra of various forms of In-fumarate-E S-32

Figure S12. IR spectra of various forms of the fumarate MOFs S-33

Figure S13. SEM images of fumarate MOFs using different synthetic temperatures S-34

Figure S14. Anisotropic T_2 relaxation in ^{71}Ga NMR spectra S-35

Figure S15. Experimental and calculated ^{71}Ga NMR spectra of Ga-fumarate-H_2O S-36

Figure S16. The comparison of pXRD patterns of various forms of In-fumarate MOFs S-37

Figure S17. ^{1}H MAS NMR spectra of various forms of In-fumarate-M S-38

Figure S18. TGA plots of various forms of In-fumarate-M S-39

Figure S19. Static ^{115}In NMR spectra of various forms of In-fumarate MOFs S-40

Table S2. Experimentally determined ^{115}In NMR parameters of various forms of In-fumarate S-40

Table S3. Measured BET surface areas of Ga-fumarate S-41

Table S4. Measured BET surface areas of In-fumarate S-41

Figure S20. ^{69}Ga, ^{71}Ga, and ^{115}In NMR spectra of activated and CO_2-loaded fumarate MOFs S-42

Figure S21. ^{27}Al NMR spectra of activated and CO_2 loaded Al-fumarate S-43

Table S5. ^{69}Ga and ^{71}Ga NMR parameters of activated and CO_2-loaded Ga-fumarate S-43

Table S6. ^{115}In NMR parameters of activated and CO_2-loaded In-fumarate S-43

Figure S22. Static ^{13}C CP SSNMR spectra of various form of In-fumarate S-44

Figure S23. Static ^{13}C CP SSNMR spectra of CO_2 loaded fumarate MOFs using various contact times S-44

Table S7. ^{13}C NMR parameters of CO_2 adsorbed within fumarate MOFs S-45

References S-46

Experimental details for materials characterization

Preparation of CO_2 loaded samples. A Schlenk line was used for sample activation and loading of CO_2 guests. A known quantity of the fumarate MOF sample was placed into the bottom of a homemade 5 mm L-shaped glass tube. A thin layer of glass wool was used as a permeable cap to secure the sample in place. The glass tube containing the sample was first attached to the Schlenk line and heated at 150 °C for 8 h under dynamic vacuum (*i.e.*, pressure < 1 mbar) to remove any residual solvents or linkers from the MOF channels. A known amount of pressurized $^{13}CO_2$ (Sigma-Aldrich, 99% ^{13}C isotope enriched, herein denoted simply as "CO_2") was then introduced to the vacuum line, and the CO_2 was allowed to occupy both the vacuum line and the glass tube containing the sample; the overall volume of this combined space is 82.7 cm^3. The bottom of the CO_2-filled glass tube containing the fumarate MOF samples was then immersed in liquid nitrogen to freeze and trap CO_2 within the sample, during which time the glass tube was flame-sealed off from the Schlenk line. The overall CO_2 loading amount is expressed by the molar ratio between CO_2 and the metal. In this study, 0.2 CO_2/metal samples were prepared and characterized by NMR.

Preparation of deuterium-exchanged Al-fumarate and Ga-fumarate samples. This procedure was performed to deuterate the bridging hydroxyl groups joining the MO_6 (M = Al, Ga, In) MOF secondary building units (SBUs). 0.10 g of the fumarate MOF was immersed in 2 mL of D_2O within a homemade 5 mm L-shaped glass tube

for two days, during which the glass tube was sealed with parafilm. The D_2O was extracted and replaced three times per day to ensure thorough deuteration of the sample. After D_2O exchange, the sample was activated and loaded with CO_2 according to the previously outlined procedure *(vide supra)*.

Powder X-ray diffraction (pXRD). All pXRD patterns for routine characterization were acquired using an Inel CPS Powder Diffractometer operating with Cu $K\alpha$ radiation (λ = 1.5406 Å). Reflections were collected at 2θ-values ranging between 5 and 120 ° using an increment of 0.02 °. The pXRD patterns for Rietveld refinement of Ga-fumarate were acquired using synchrotron data obtained from beamline 08B1-1 at the Canadian Light Source in Saskatoon, Canada, which employed X-rays with an energy of 18 keV (λ = 0.68880Å). 08B1-1 is a bending magnet beamline utilizing a Si (111) double crystal monochromator for energy selection and a 2D Rayonix MX300HE detector (active area 300 × 300 mm^2) for data acquisition.

The 2D PXRD patterns were calibrated and integrated using the GSASII software package.[1] The sample–detector distance, detector centering, and tilt were calibrated using a lanthanum hexaboride (LaB_6) standard reference material (NIST SRM 660a LaB_6) and the calibration parameters were applied to all patterns. After calibration, the 2D patterns were integrated to obtain standard 1D powder diffraction patterns. A pattern collected from an empty Kapton capillary, acquired using the same conditions, was subtracted from the sample data during integration.

Rietveld refinement of Ga fumarate MOF structure. Rietveld refinement[2] of the gallium fumarate MOF structure was performed using the program TOPAS Academic 6.[3] Diffraction peak shapes were modelled by a pseudo-Voigt function, while the background was described by a 6th degree Chebyshev polynomial. The structure was refined in a monoclinic space group *I2/a*. The asymmetric unit contained one Ga atom located on a special position, one bridging hydroxyl anion, half a fumarate anion, as well as two water oxygen atoms. During the refinement, the gallium atom remained fixed at the special position, the bridging hydroxyl was allowed to move along the y-coordinate, while the fumarate fragment and water molecules were allowed to refine freely. The fumarate linker was described by a rigid body, with geometry taken from the structure optimized in CASTEP.

BET surface area and CO_2 adsorption isotherm measurements. BET surface areas of each sample were measured at a temperature of 77 K using a Micromeritics ASAP 2020 Surface Area and Porosity Analyzer instrument, operating with nitrogen (N_2) as the probe gas. CO_2 adsorption isotherms were measured at a temperature of 273 K using the same instrument. Prior to measuring the BET surface areas and CO_2 adsorption isotherms, all fumarate MOF samples were degassed under dynamic vacuum (< 1 mbar) at 150 °C for 8 hours using the same instrument. **Note:** a very small dip in N_2 adsorption within Al-fumarate was observed and its origin is not currently known since no leaks were detected before measurement.

Fourier Transform Infrared (FTIR) spectroscopy. All Ga-fumarate and

In-fumarate samples were first packed into a diamond anvil cell (DAC) at room temperature in a glovebox under N_2 atmosphere. A customized IR micro-spectroscopy system was used for all IR absorption measurements, along with a commercial Fourier transform infrared (FTIR) Bruker Vertex 80v spectrometer equipped with a Globar mid-IR light source. The micro-IR system was operated under a vacuum of < 5 mbar to ensure H_2O removal from the sample. The IR beam was focused onto the sample in the DAC, and the transmitted IR beam was collected using a wide-band mercury cadmium telluride (MCT) detector equipped with a ZnSe window that permitted measurements in the spectral range between 600 and 12000 cm^{-1}.

SSNMR experiments. All experiments at a magnetic field of 9.4 T were performed using a Varian InfinityPlus wide-bore NMR spectrometer ($\nu_0(^{13}C)$ = 100.1 MHz, $\nu_0(^{1}H)$ = 399.5 MHz), while all experiments at a magnetic field of 21.1 T were performed using a Bruker Avance II NMR spectrometer ($\nu_0(^{13}C)$ = 226.3 MHz, $\nu_0(^{1}H)$ = 900.1 MHz) located at the National Ultrahigh-Field NMR Facility for Solids in Ottawa, ON, Canada. ^{1}H MAS and ^{13}C CP/MAS NMR experiments at 9.4 T were carried out using a 4 mm HXY Varian/Chemagnetics MAS probe, with all samples packed into 4.0 mm (outer diameter (o.d)) ZrO_2 rotors. All static ^{13}C NMR experiments targeting $^{13}CO_2$ adsorbed in the fumarate MOFs were carried out at 9.4 T on the same spectrometer using a Varian/Chemagnetics 5 mm HX static probe. ^{1}H MAS NMR experiments at 21.1 T were performed using a 2.5 mm H/X MAS Bruker probe with all samples

packed into 2.5 mm (o. d.) ZrO_2 rotors. More specific details on each type of NMR experiment performed are provided below.

All ^{13}C chemical shifts were referenced to tetramethylsilance (TMS) by using adamantane as a secondary reference (δ_{iso} = 38.52 ppm for the high-frequency resonance),[4] and ^{1}H chemical shifts were referenced to TMS using adamantane as a secondary reference (δ_{iso} = 1.85 ppm).[4] A Varian VT temperature control unit was used to adjust the temperature for all VT experiments. All temperatures were measured to ± 2 K and were calibrated using the known ^{207}Pb chemical shift of solid $Pb(NO_3)_2$ across the experimental temperature range.[5]

^{13}C cross-polarization (CP)/MAS NMR experiments. All ^{13}C CP/MAS spectra of the fumarate MOFs were acquired at a magnetic field of 9.4 T. The ^{1}H 90 ^{o} pulse employed was 4.4 μs and a spectral width of 50 kHz was used, along with a mixing time of 3 ms and a pulse delay of 2 s. All ^{13}C CP/MAS SSNMR experiments were performed employing a ^{1}H decoupling field of 50 kHz and Hartmann–Hahn matching fields of 48 kHz on the ^{13}C channel and 50 kHz on the ^{1}H channel. The MAS spinning frequency used for all ^{13}C CP/MAS experiments was 14 kHz.

^{1}H MAS NMR experiments. All ^{1}H MAS spectra of Ga-fumarate were acquired at a magnetic field of 9.4 T, using a standard Bloch-decay (*i.e.*, one-pulse) experiment along with a spectral width of 150 kHz. The ^{1}H 90 ° pulse length was 4.4 μs long, the pulse delay was 3 s, and the spinning frequency was 14 kHz. All ^{1}H MAS

spectra of In-fumarate were acquired at a magnetic field of 21.1 T using a rotor-synchronized echo experiment of the form $\pi/2 - \tau_1 - \pi/2 - \tau_2$ - acq, along with a spectral width of 250 kHz, a ^{1}H 90 ° pulse length of 2.5 μs, a pulse delay of 10 s, and a spinning frequency of 31.25 kHz.

Static ^{13}C NMR of adsorbed CO_2. All static ^{13}C NMR spectra were acquired using the DEPTH-echo pulse sequence[6] at a magnetic field of 9.4 T, employing a ^{13}C 90 ° pulse length of 3.1 μs and a 180 ° pulse length of 6.2 μs. The optimized ^{13}C pulse delay between scans was determined to be 7.5 s for all fumarate MOFs. At experimental temperatures below 193 K, the optimized ^{13}C pulse delay for all samples increased to 15 s. All static spectra were acquired using a ^{1}H decoupling field of 81 kHz. For static ^{1}H-^{13}C CP experiments at 133 K, 10 ms contact times (CT) were employed. All static ^{13}C NMR spectra were referenced to the high-frequency resonance of carbon in liquid ethanol, which is located at 58.05 ppm with respect to TMS.[7]

^{69}Ga and ^{71}Ga NMR experiments at 21.1 T. All ^{69}Ga and ^{71}Ga NMR experiments were performed at a magnetic field of 21.1 T, using a Bruker Avance II NMR spectrometer located at the National Ultrahigh-Field NMR Facility for Solids in Ottawa, ON, Canada. A home-built 5 mm HX static probe was used to acquire all ^{69}Ga and ^{71}Ga spectra (ν_0(^{69}Ga) = 216.0 MHz, ν_0(^{71}Ga) = 274.4 MHz). Both ^{71}Ga and ^{69}Ga NMR shifts were referenced to water-solvated Ga^{3+} using a solution of 1 M $Ga_2(SO_4)_3$ (δ_{iso} = 0).[8] All spectra were acquired using a modified 90 ° - 180 ° quadrupolar-echo

pulse sequence of the form ($\pi/2$ - τ_1 - $\pi/2$ - τ_2 - acq) with a spectral width of 2000 kHz. A 90 ° CT-selective pulse length of 2 μs was used to acquire ^{71}Ga spectra and a 90 ° CT-selective pulse length of 3 μs was used to acquire ^{69}Ga spectra. Pulse delays of 0.5 s were sufficient for the acquisition of ^{71}Ga and ^{69}Ga spectra. Due to the relatively large quadrupole moment of ^{69}Ga, powder pattern breadths were too large to properly excite and acquire in a single experiment. The overall ^{69}Ga powder pattern was constructed by co-adding two or more frequency-stepped individual sub-spectra in technique known as piecewise acquisition or variable-offset cumulative spectrum (VOCS).[9]

^{115}In NMR experiments at 21.1 T. ^{115}In NMR experiments were performed at a magnetic field of 21.1 T (ν_0(^{115}In) = 197.2 MHz). A home-built 5 mm HX static probe was used and ^{115}In NMR chemical shifts was referenced using 0.1 M $In(NO_3)_3$ in 0.5 M HNO_3 (δ_{iso} = 0 ppm).[8] All spectra were acquired using a modified 90 ° - 180 ° quadrupolar-echo pulse sequence of the form ($\pi/2$ - τ_1 - $\pi/2$ - τ_2 - acq) with a spectral width of 5000 kHz, 90 ° CT-selective pulse length of 0.5 μs, and pulse delay of 0.25 s. Due to the large quadrupole moment of ^{115}In, the ^{115}In powder patterns were of considerable breadth and required the acquisition and summation of several individual piecewise spectra using the VOCS[9] protocol.

Density-functional theory (DFT) calculations. Plane-wave DFT calculations are commonly used to complement experimental investigations of NMR parameters in systems incorporating a variety of nuclei and structural motifs.[10] In this study,

calculations were focused on the Ga-fumarate system, and were performed using the CASTEP software package.[11-12] The geometry optimization was performed with all unit cell parameters taken from the refined crystal structure of Ga-fumarate-H_2O. The generalized gradient approximation (GGA) within the Perdew–Burke–Ernzerhof (PBE) paremeterization[13] combined with Grimme D2 dispersion correction[14] were employed. A basis set containing plane-waves up to 750 eV was used, and the first Brillouin zone was sampled with a 0.03 $Å^{-1}$ *k*-point spacing. The $^{69/71}$Ga electric field gradient (EFG) and chemical shift (CS) tensor parameters were calculated using the NMR module.[15-16] The gauge-including projector-augmented wave (GIPAW) method was used with on-the-fly generated pseudopotentials and plane-wave basis sets.[11] The plane-wave cutoff was increased to 1000 eV, while the scales of standard and fine FFT grids were set to 2 and 3, respectively. Calculations of the ^{115}In NMR parameters for In-fumarate were not performed due to the unknown nature of the crystal structure; direct substitution of In within the refined Ga-fumarate-H_2O structure produced values that were a very poor match to experimental measurements (not shown).

Spectral simulation software. The WSolids[17] computer software was used to perform analytical simulations of experimental NMR spectra in order obtain all ^{69}Ga and ^{71}Ga NMR parameters as well as the observed or apparent ^{13}C NMR parameters, while the QUEST[18] software was used to simulate ^{115}In spectra due to its relatively large quadrupolar interaction. The EXPRESS[19] software was used to simulate the

effects of CO_2 dynamics on ^{13}C NMR powder patterns and to extract CO_2 motional information.

Chemical shift (CS) tensor convention. The CS interaction is modeled by a trace second-rank tensor defined by three orthogonal components, δ_{11}, δ_{22}, and δ_{33}, which are ordered such that $\delta_{11} \geq \delta_{22} \geq \delta_{33}$. The isotropic chemical shift, δ_{iso}, is the average of all three tensor components and is defined as $\delta_{iso} = (\delta_{11} + \delta_{22} + \delta_{33})/3$. The span of the CS tensor, Ω, denotes the breadth of the powder pattern and is the difference between the largest and smallest tensor components, where $\Omega = \delta_{11} - \delta_{33}$. The skew (κ) describes the axial symmetry of the CS tensor and is defined as $\kappa = 3(\delta_{22} - \delta_{iso})/\Omega$. Values for κ range from −1 to +1, with either limit representing an axially symmetric CS tensor.

Electric field gradient (EFG) tensor convention. The EFG can be modeled by a traceless second rank tensor with orthogonal components V_{11}, V_{22}, and V_{33}, which are ordered such that $|V_{33}| \geq |V_{22}| \geq |V_{11}|$. The quadrupolar interaction (QI) describes the interaction between the electric quadrupole moment of the nucleus and the surrounding EFG, which arises from the local nuclear surroundings such as chemical bonds, point charges, etc. The magnitude of the QI can be defined using the quadrupolar coupling constant C_Q, and the axial symmetry of the EFG tensor is described using the asymmetry parameter η_Q. C_Q describes the local spherical symmetry of the ground-state electronic environment about the nucleus, and is calculated as $C_Q = eQV_{33}/h$. A large C_Q value corresponds to a lower degree of local

spherical symmetry and relatively broader powder patterns; in contrast, smaller C_Q values represent a higher degree of spherical symmetry and narrower powder patterns. η_Q is linked to the axial symmetry of the EFG tensor, and by extension the axial symmetry of the local electronic environment, and is defined such that $\eta_Q = (V_{11} - V_{22})/V_{33}$. η_Q can range in value from 0 to 1, with decreased η_Q values corresponding to a more axially symmetric EFG tensor. The Euler angles α, β, and γ are used to describe the relative orientation of the EFG and CS tensors according to the Rose convention.[20]

Thermogravimetric analysis (TGA). TGA analysis was performed under dry N_2 flow using a Mettler Toledo TGA/SDTA851e instrument. A temperature range between 25 °C and 800 °C and a heating rate of 10 °C /min were employed. For each TGA experiment, ca. 5-10 mg of the sample was placed within a ceramic crucible.

SEM analysis. All morphological analysis of Ga-fumarate was performed using a LEO (Zeiss) 1540XB FIB/SEM instrument and all SEM analysis of In-fumarate samples was performed using a LEO (Zeiss) 1530 SEM instrument.

Elemental analysis (EA). The elemental analysis of *as-made* Ga-fumarate (Ga-fumarate(*as*)) and *as-made* In-fumarate-E (In-fumarate*(as)*) was carried out using an ECS 4010 CHNOS analyzer from Costech, located at the Université de Montréal in Montréal, Québec, Canada.

Additional results and discussion

Thermogravimetric analysis (TGA) experiments. TGA was used in order to determine the amount of adsorbed guests within Ga-fumarate(*as*), and to confirm the chemical formula of Ga-fumarate(*as*) that was determined from elemental analysis.

The TGA results of Ga-fumarate(*as*) are pictured in Figure S6(a). Three different weight losses are evident upon heating the Ga-fumarate(*as*) sample. The first weight loss of 4 % occurred slightly below 100 °C, and corresponds to the loss of H_2O from the Ga-fumarate MOF channels. A second weight loss event of 19 % occurred between 150 °C and 250 °C, and can be assigned to guest DMF molecules being purged from the MOF pores. The third and final weight loss takes place just below 400 °C and accounts for a 33 % loss of the initial MOF weight; this substantial loss signifies that the MOF has decomposed. From TGA experiments and the corresponding weight loss assignments, the calculated chemical formula of Ga-fumarate(*as*) was determined to be $Ga(OH)(C_4H_2O_4)\cdot 0.68DMF\cdot 0.58H_2O$, which is similar to the calculated chemical formula of $Ga(OH)(C_4H_2O_4)\cdot 0.685DMF\cdot 0.581H_2O$ based on elemental analysis (C: 27.51 %, H: 3.43 %, N: 3.67 %). The TGA plot of activated Ga-fumarate (Figure S6(b)) shows a single weight loss at 400 °C corresponding to MOF decomposition; the lack of any minor weight losses at lower temperatures indicates that the activation process successfully removed all guest molecules from the channels of Ga-fumarate. A sample of activated Ga-fumarate

exposed to air (20 % relative humidity, r.h.) for 3 days was also examined using TGA (Figure S6(c)), revealing one weight loss at ca. 100 °C denoting the removal of adsorbed H_2O molecules, and another weight loss beginning at 400 °C corresponding to decomposition of the MOF. These TGA results indicate that the empty channels of activated Ga-fumarate readily adsorb water from the atmosphere to form Ga-fumarate-H_2O. The calculated ratio of H_2O/Ga in Ga-fumarate-H_2O is 3.5 (*i.e.*, Ga-fumarate·3.5H_2O or Ga(OH)($C_4H_2O_4$)·3.5H_2O), which is the same ratio found for Al-fumarate-H_2O.[21]

The TGA results of In-fumarate-E(*as*) are illustrated in Figure S7(a). In this instance, only two weight losses were observed. The first weight loss of 17 % around 150 °C can be assigned to guest ethanol and water molecules being purged from the MOF channels. The second weight loss of 31 % just below 400 °C corresponds to decomposition of the MOF. Based on these TGA experiments and weight loss assignments, along with the elemental analysis results (C: 20.79 %, H: 1.99 %), the calculated chemical formula of In-fumarate-E(*as*) was determined to be In(OH)($C_4H_2O_4$)·0.57(CH_3CH_2OH)·1.35(H_2O). The TGA plot of activated In-fumarate-E (Figure S7(b)) is similar to that of activated Ga-fumarate (Figure S6(b)). Due to prior removal of guest ethanol and water, only a single weight loss at 400 °C was observed from activated In-fumarate-E, which corresponds to MOF decomposition. The TGA plot of activated In-fumarate-E after exposure to air (20 % r.h.) for 3 days indicates that adsorption of H_2O occurred, as evidenced by a weight loss of 18 % at ca. 100 °C

(Figure S7(c)). The calculated H_2O/In ratio within In-fumarate-E-H_2O is 3.0, yielding a formula of In-fumarate-3.0H_2O or In(OH)($C_4H_2O_4$)·3.0H_2O; notably, the H_2O/metal ratio of In-fumarate-E-H_2O is smaller than those of Al- and Ga-fumarate. The relatively smaller amount of water within In-fumarate-E is due to the smaller free space available within this MOF, which is caused by the larger atomic size of In versus Ga and Al. The amount of adsorbed water within the fumarate MOFs follows the trend: Al-fumarate ≥ Ga-fumarate > In-fumarate.

^{1}H MAS and ^{13}C CP/MAS NMR experiments. NMR experiments targeting ^{1}H and ^{13}C nuclei in Ga-fumarate(*as*) were used to characterize and identify guest molecules, as well as to confirm the existence of key MOF structural features. All ^{1}H MAS and ^{13}C CP/MAS NMR experiments on Ga-fumarate were acquired at a magnetic field of 9.4 T. The presence of DMF guests in Ga-fumarate(*as*) was confirmed by ^{1}H MAS and ^{13}C CP/MAS NMR experiments, shown in Figures S8(b) and Figure S9(b)). The removal of guest DMF and H_2O after the activation process was verified *via* ^{1}H MAS and ^{13}C CP/MAS NMR spectra of activated Ga-fumarate (Figure S8(c) and Figure S9(c)). The adsorption of H_2O within the empty channels of Ga-fumarate to form Ga-fumarate-H_2O was also confirmed by ^{1}H NMR experiments (Figure S8(d) and Figure S9(d)). The ^{1}H resonance corresponding to bridging –OH groups could not be clearly identified in NMR spectra of Ga-fumarate(*as*) and Ga-fumarate-H_2O due to spectral overlap with more intense resonances (Figure S8(b) and (d)).

NMR experiments on In-fumarate-E were also performed to confirm the

presence of specific structural features. ^{1}H MAS NMR experiments at 21.1 T with a fast spinning frequency of 31.25 kHz were employed to obtain high-resolution ^{1}H NMR spectra, while ^{13}C CP/MAS NMR spectra of In-fumarate-E samples were acquired at 9.4 T. The presence of ethanol within In-fumarate-E(*as*) was first confirmed by ^{1}H MAS and ^{13}C CP/MAS NMR experiments (Figure S10(b) and Figure S11(b)). After activation, the ^{13}C CP/MAS NMR spectrum (Figure S11 (c)) and TGA (Figure S7(b)) of In-fumarate-E suggest that ethanol guests were entirely removed from the MOF, however, the ^{1}H MAS NMR experiments at 21.1 T (Figure S10(c)) reveal that a small quantity of ethanol remains within the MOF. The presence of unremoved ethanol in activated In-fumarate-E was confirmed using IR spectroscopy, as the remaining ethanol molecules give rise to the broad O-H stretch that ranges from 3050 to 3570 cm^{-1} (Figure S12(d)). The adsorption of H_2O within the empty channels of In-fumarate-E to form In-fumarate-E-H_2O was verified by ^{1}H NMR spectra (Figure S10(d)).

Infrared spectroscopy. The H_2O and DMF guests in Ga-fumarate(*as*) can be observed using IR spectroscopy (Figure S12(a)), as the O-H stretch gives rise to the broad absorption from 2700 to 3700 cm^{-1}; the O-H stretch of the bridging hydroxyl group is visible as a shoulder at ca. 3670 cm^{-1}. The removal of guest DMF and H_2O molecules during the activation process is evident in the IR spectrum of activated Ga-fumarate (Figure S12(b), as is the subsequent adsorption of water in empty Ga-fumarate to form Ga-fumarate-H_2O (Figure S12(c)). The IR specta of activated

In-fumarate-E and In-fumarate-M are also shown in Figure S12(d) and (e), respectively.

SEM imaging. The SEM images (Figure S13(a)) provide insight into how the particle size and morphology of Ga-fumarate samples are influenced by different synthetic temperatures. When a temperature of 60 °C is employed during synthesis, the Ga-fumarate product forms as jagged, somewhat square- or cube-shaped crystals measuring less than 2 μm across, which exhibit a rough surface (Figure S13(a)). When the synthesis temperature is increased to 80 °C, smooth plate-shaped crystals of Ga-fumarate smaller than 2 μm are produced (Figure S13(a)). After performing the synthesis at 180 °C, the resulting particle size of the product is < 100 nm and no regular crystal shape is apparent (Figure S13(a)).

The particle size and morphology of In-fumarate-E differs from those of Ga-fumarate. At 40 °C, the In-fumarate-E product is formed as irregularly-shaped crystals that are generally less than 1 μm in size (Figure S13(b)). In-fumarate-E is formed as needle-shaped crystals when a synthesis temperature of 80 °C is used (Figure S13(b)). When the synthesis temperature is increased to 120 °C, the particle size of In-fumarate-E is < 100 nm and no regular crystal shape is apparent (Figure S13(b)); a very similar observation was made for Ga-fumarate at a synthesis temperature of 180 °C. The SEM images also indicate that different morphologies have been obtained in In-fumarate-M, when $–OCH_3$ groups have been introduced into the framework (Figure S13(c)). At synthesis temperatures of 20 °C and 80 °C, the

In-fumarate-M MOF is produced as various types of irregularly shaped particles that are under ca. 1 μm in size, while an increased synthesis temperature of 120 °C results in very large, irregularly shaped particles with sizes in the realm of 300-400 nm.

Static ^{69}Ga, ^{71}Ga, and ^{115}In NMR experiments of CO_2 loaded Ga-fumarate and In-fumarate MOFs. Static ^{69}Ga and ^{71}Ga SSNMR spectra of activated and then CO_2-loaded Ga-fumarate (herein termed "CO_2-loaded Ga-fumarate") were acquired at 21.1 T to investigate the influence of CO_2 adsorption on Ga metal centers in this MOF, and additionally to investigate any Ga-CO_2 interactions that may be present. The ^{69}Ga and ^{71}Ga SSNMR spectra of activated and CO_2 loaded Ga-fumarate are shown in Figure S20(a) and (b), with associated NMR parameters found in Table S5. The ^{69}Ga and ^{71}Ga SSNMR spectra of the empty activated Ga-fumarate and CO_2-loaded Ga-fumarate samples are nearly identical. The very similar NMR parameters between both samples indicate that the coordination environment of Ga centers is unchanged upon CO_2 adsorption, Ga plays little or no direct role in CO_2 adsorption, and the CO_2-MOF interaction is too weak to significantly distort or otherwise influence the local GaO_6 environment within Ga-fumarate. This finding stands in contrast to the pronounced effect that H_2O adsorption has on ^{69}Ga and ^{71}Ga NMR spectra; the relatively stronger H_2O-MOF binding gives rise to distortions in the GaO_6 octahedra and larger $C_Q(^{69}Ga)$ and $C_Q(^{71}Ga)$ values, while the relatively weaker CO_2-MOF interaction does not significantly distort GaO_6 octahedra or modify the ^{69}Ga and ^{71}Ga NMR parameters.

The metal centers in CO_2-loaded Al-fumarate and In-fumarate were also examined using solid-state NMR. A conclusion similar to CO_2-loaded Ga-fumarate arises from the identical static ^{27}Al NMR spectra of empty activated Al-fumarate and CO_2-loaded Al-fumarate (Figure S21): CO_2 has little effect on the local Al environment and does not bind directly to Al. The ^{115}In NMR spectra of activated and CO_2 loaded In-fumarate-E and In-fumarate-M are shown in Figure S20(c) and (d), respectively, with associated NMR parameters listed in Table S6. There is no significant change in the ^{115}In NMR powder pattern lineshapes and NMR parameters of activated In-fumarate-E and –M before and after CO_2 adsorption, indicating that CO_2 has little effect on the local indium environment and does not bind directly to the metal.

Since the metal centers do not play a direct role in CO_2 adsorption at room temperature, the bridging hydroxyl groups and fumarate linkers must interact with CO_2 in the fumarate MOFs. In order to further investigate the CO_2 adsorption location, static ^{13}C cross-polarized (CP) NMR experiments were performed on CO_2-loaded Al-, Ga-, and In-fumarate samples, to establish a possible connectivity between framework hydrogen atoms and the $^{13}CO_2$ carbon atoms.

Static ^{13}C CP NMR experiments of CO_2 loaded fumarate MOFs to study the CO_2 binding strength. The contact time in ^{13}C CP experiments targeting adsorbed CO_2 is useful for investigating the CO_2 adsorption strength and location in the fumarate MOFs, and making comparisons versus similar MOFs such as MIL-53. Since a long contact time is associated with more distance between ^{1}H and ^{13}C, while short

contact times are correlated to closer ^{1}H-^{13}C contacts, the required contact time can give some qualitative information regarding spatial proximities. In this study, a contact time of 10 ms was required to successfully transfer ^{1}H polarization from framework hydrogen atoms to the ^{13}C nuclei of adsorbed CO_2 guests (Figure S23), which hints at a rather long ^{1}H-^{13}C distance and a relatively weak ^{1}H-^{13}C interaction strength.

In contrast, ^{13}C CP NMR experiments examining $^{13}CO_2$ in MIL-53 exhibited successful polarization transfer to $^{13}CO_2$ when contact times of 0.5 and 5 ms were used,[6] indicating that a significantly shorter ^{1}H-^{13}C distance is present versus the fumarate MOFs, and suggesting that CO_2 interacts relatively more strongly with the MIL-53 MOF.

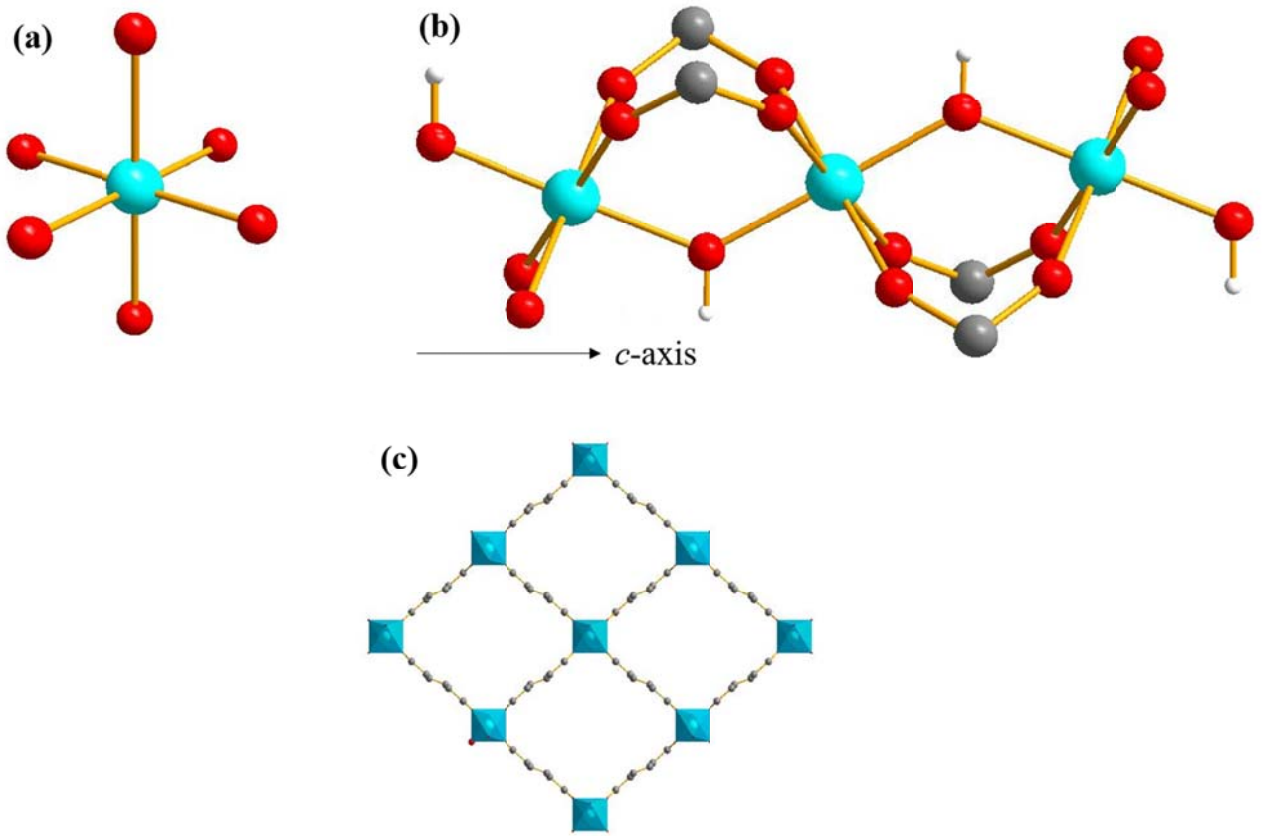

Figure S1. The octahedral $MO_4(OH)_2$ secondary building unit (SBU) of the MIL-53 MOF is shown in (a). The chain formed by the SBUs along the crystallographic *c* axis is shown in (b); these chains are interconnected by benzenedicarboxylate (BDC) linkers to create the one-dimensional rhombic channels shown in (c). The colors red, grey, white and blue correspond to oxygen, carbon, hydrogen and the metal center, respectively. (Reproduced from ref [6] with permission of the PCCP Owner Societies.)

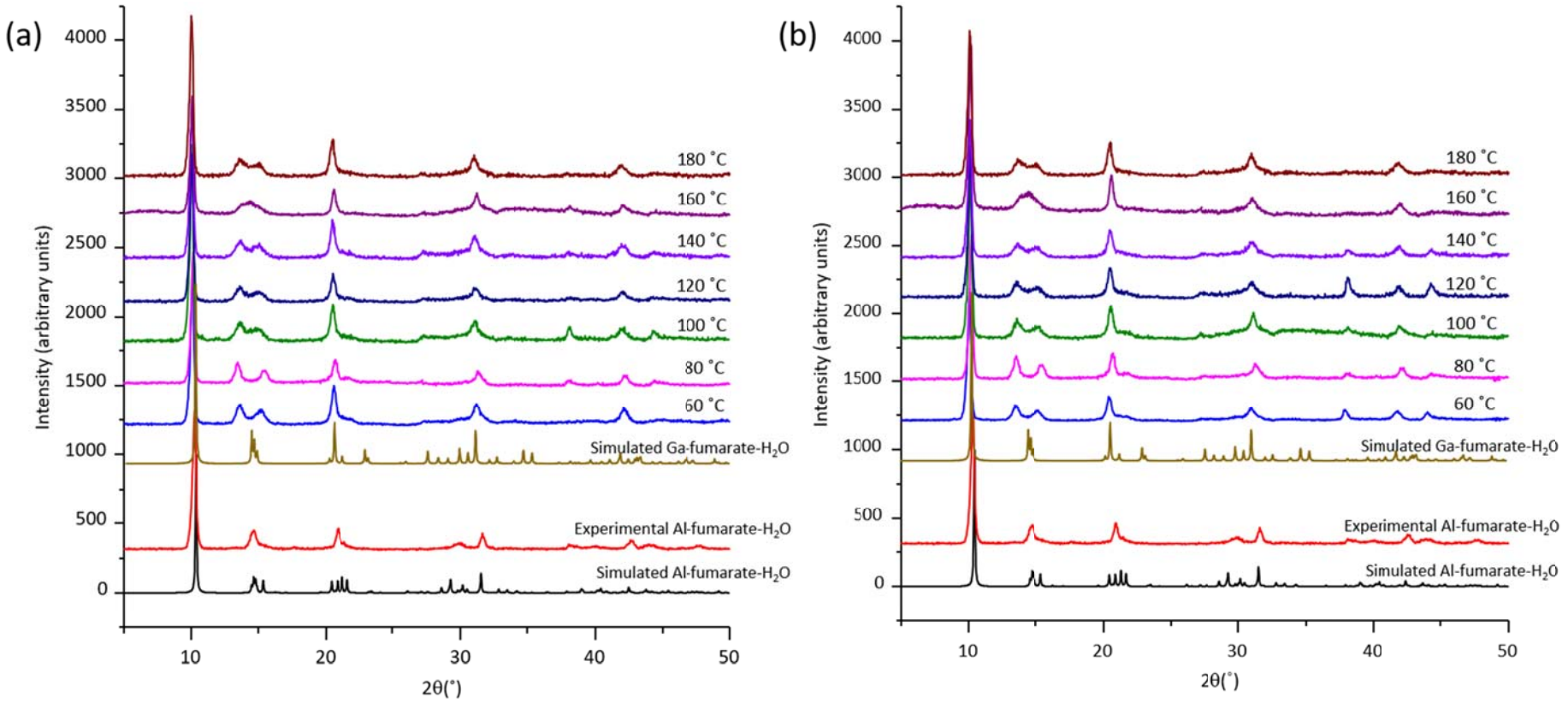

Figure S2. The experimental pXRD patterns of as-made Ga-fumarate synthesized at temperatures ranging from 60 °C to 180 °C are shown in (a) and (b), along with experimental and simulated Al-fumarate-H_2O and simulated Ga-fumarate-H_2O pXRD patterns; all simulations were calculated from the corresponding crystal structures. In (a), the Ga-fumarate MOF was synthesized using a 1:1 molar ratio of Ga in $Ga(NO_3)_3 \cdot xH_2O$ to fumaric acid reagents, while in (b), the Ga-fumarate sample was synthesized using a 1:2 molar ratio of $Ga(NO_3)_3$ to fumaric acid. For the samples synthesized at higher temperatures, the pXRD patterns exhibit reduced signal-to-noise ratios and the reflections are broadened due to lower sample crystallinity. Note the x-axis has been truncated to exclude very low angles.

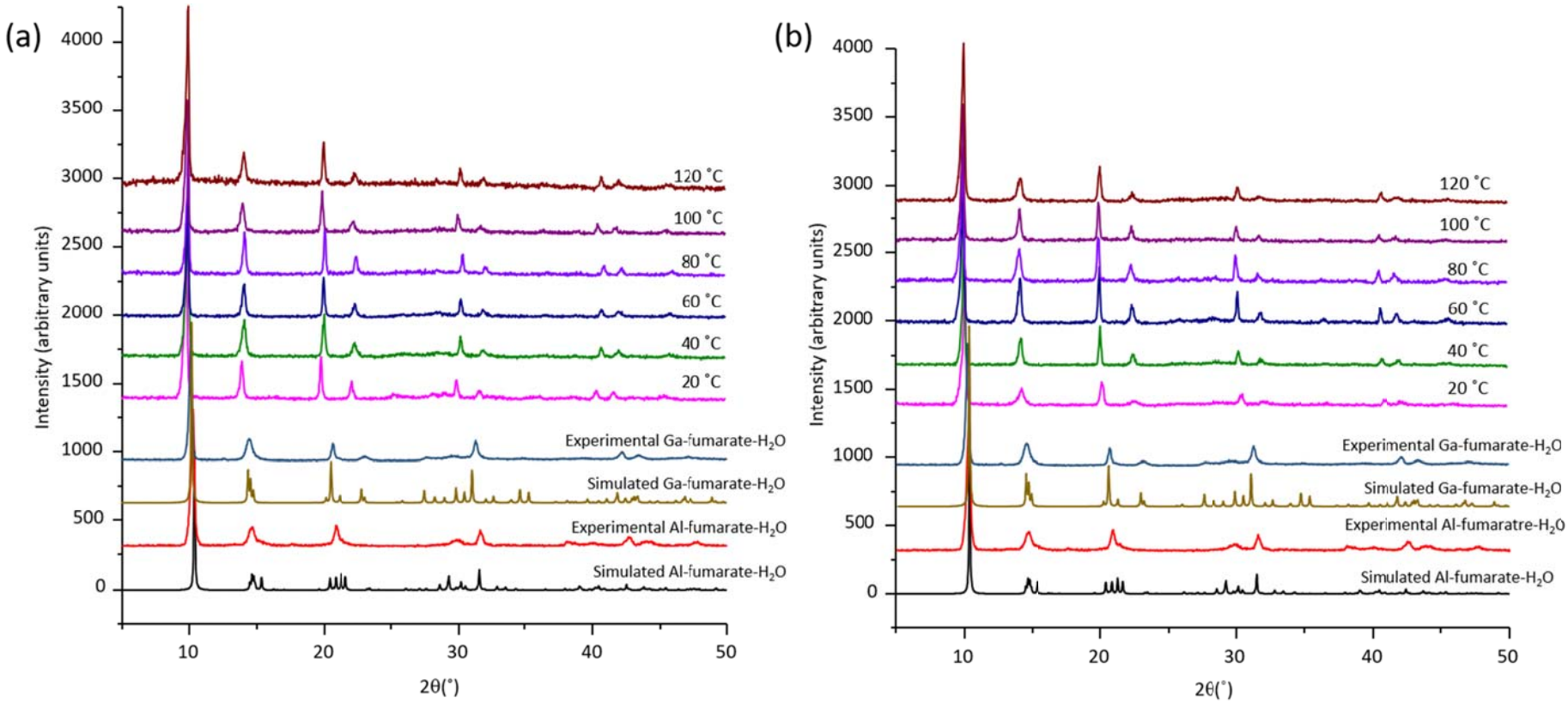

Figure S3. The experimental pXRD patterns of as-made In-fumarate-E synthesized at temperatures ranging from 20 °C to 120 °C are shown in (a) and (b), along with experimental and simulated Al-fumarate-H_2O and Ga-fumarate-H_2O pXRD patterns; all simulations were calculated from the corresponding crystal structures. In (a), the In-fumarate-E MOF was synthesized using a 1:1 molar ratio of In within $In(NO_3)_3 \cdot xH_2O$ to fumaric acid reagents, while in (b), the In-fumarate-E sample was synthesized using a 1:2 molar ratio of indium within $In(NO_3)_3 \cdot xH_2O$ to fumaric acid. For the samples synthesized at higher temperatures, the pXRD patterns exhibit reduced signal-to-noise ratios and the reflections are broadened due to lower sample crystallinity. Note the x-axis has been truncated to exclude very low angles.

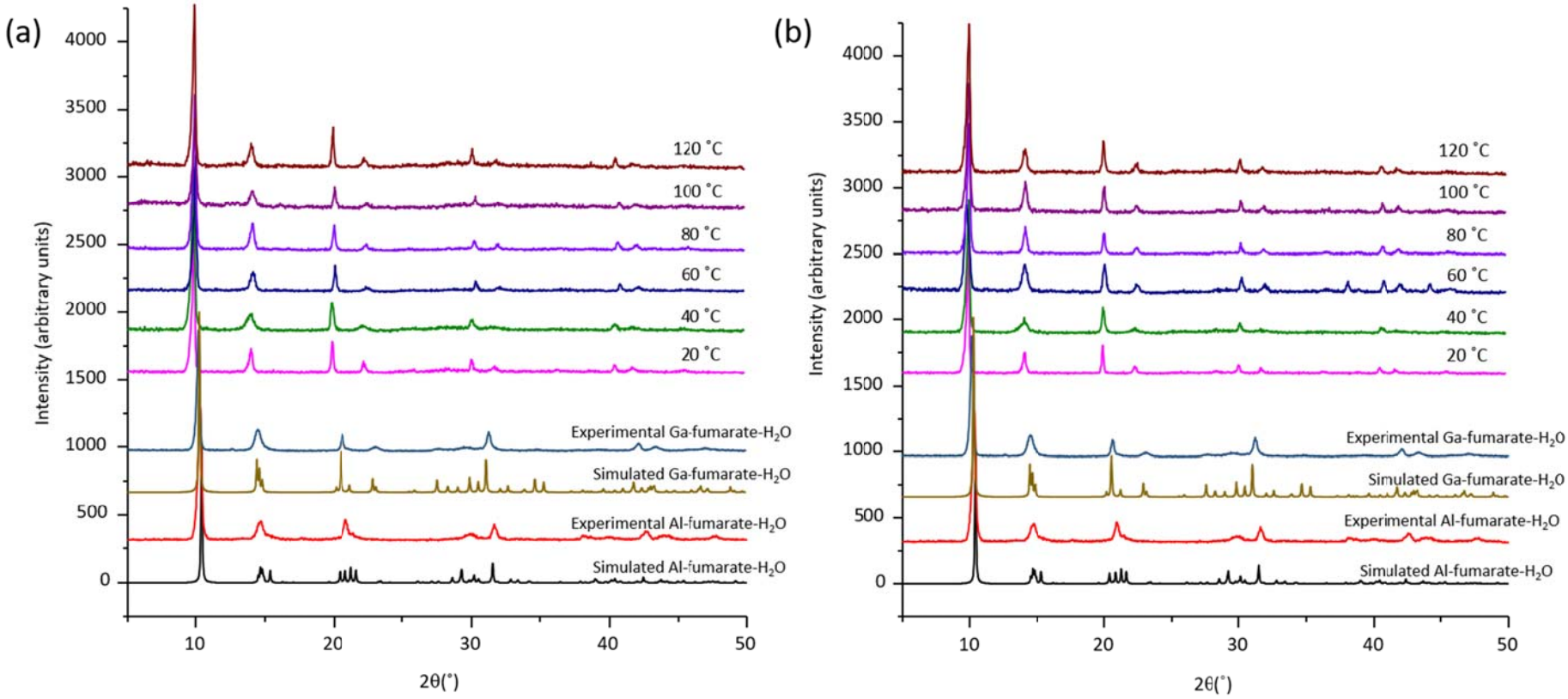

Figure S4. The experimental pXRD patterns of as-made In-fumarate-M synthesized at temperatures ranging from 20 °C to 120 °C are shown in (a) and (b), along with experimental and simulated Al-fumarate-H_2O and Ga -fumarate-H_2O pXRD patterns; all simulations were calculated from the corresponding crystal structures. In (a), the In-fumarate-M MOF was synthesized using a 1:1 molar ratio of indium within $In(NO_3)_3 \cdot xH_2O$ to fumaric acid, while in (b), the In-fumarate-M sample was synthesized using a 1:2 molar ratio of indium within $In(NO_3)_3 \cdot xH_2O$ to fumaric acid. For the samples synthesized at higher temperatures, the pXRD patterns exhibit reduced signal-to-noise ratios and the reflections are slightly broadened due to lower sample crystallinity. Note the x-axis has been truncated to exclude very low angles.

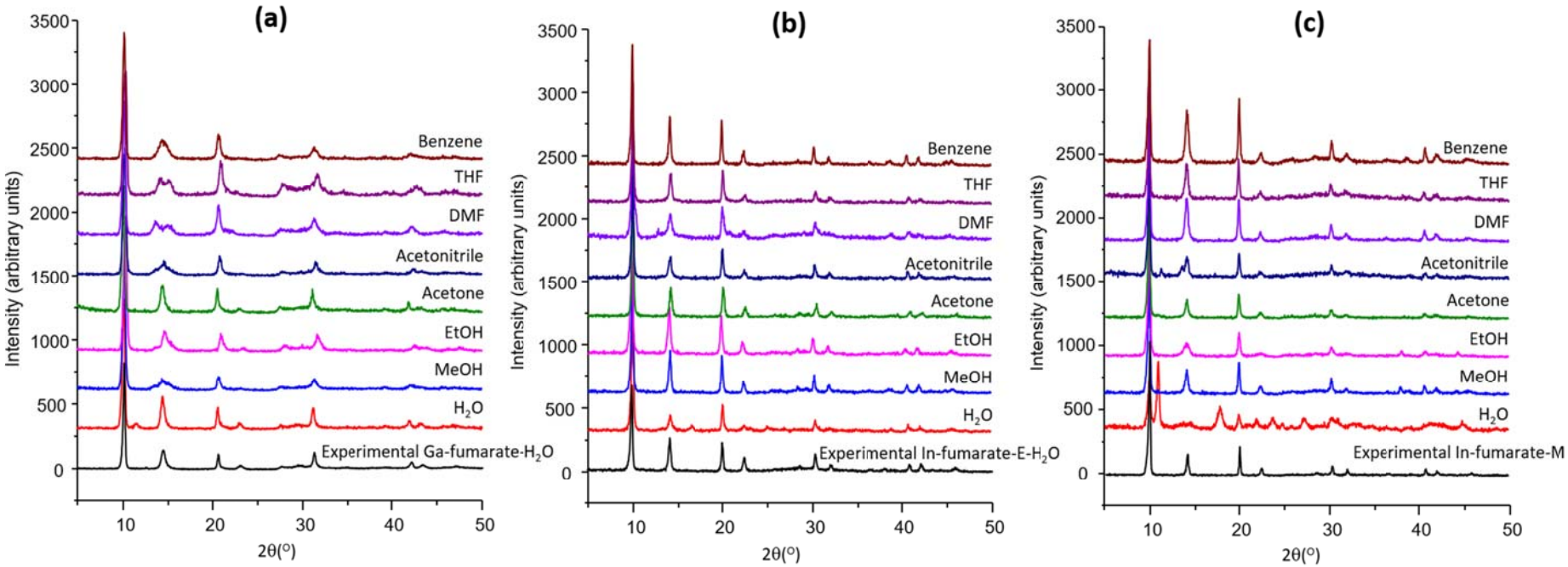

Figure S5. The pXRD patterns of activated (a) Ga-fumarate, (b) In-fumarate-E, and (c) In-fumarate-M MOF samples obtained after immersion in various solvents for 7 days. The In-fumarate-M MOF appears to have decomposed after H_2O treatment, while the rest of MOFs retain both their general structure and high degree of crystallinity after solvent treatment. Note the x-axis is truncated to exclude very low angles.

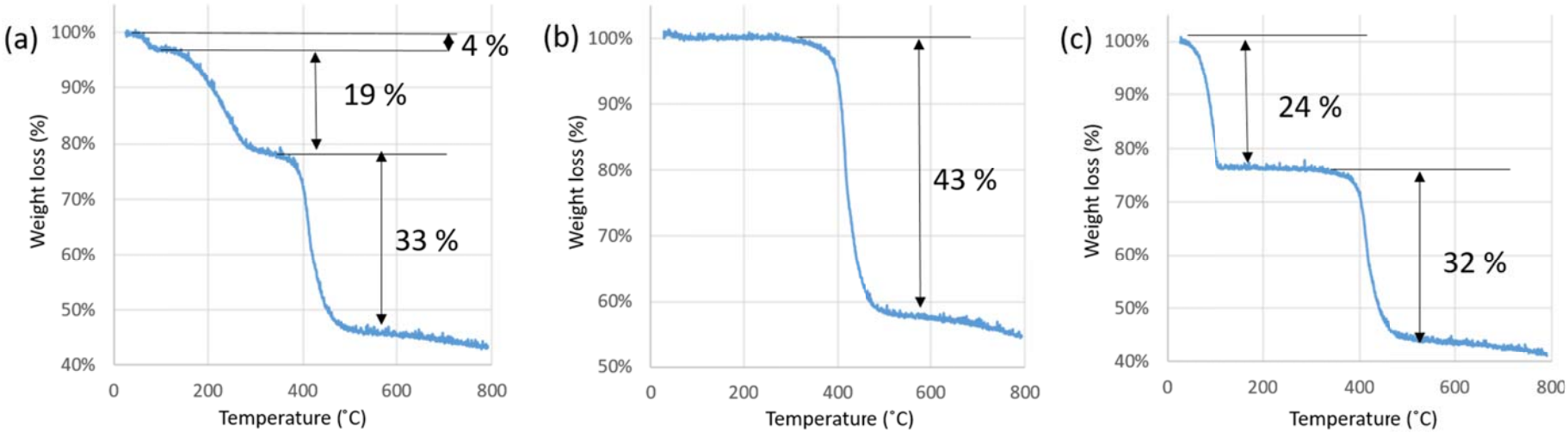

Figure S6. Thermogravimetric analysis (TGA) plots of (a) Ga-fumarate(*as*) synthesized at 80 °C; (b) Ga-fumarate after activation under dynamic vacuum at 150 °C for 8 h; and (c) Ga-fumarate after activation followed by exposure to air (20 % r.h.) for 3 days to adsorb water (*i.e.*, Ga-fumarate-H_2O). Note the difference in y-axis scale between (b) and (a)/(c).

Table S1. The experimentally determined and calculated ^{69}Ga and ^{71}Ga NMR parameters of activated Ga-fumarate and Ga-fumarate-H_2O. The experimentally determined NMR parameters of activated (large-pore) Ga-MIL-53 are listed for comparison with Ga-fumarate due to the similar SBU geometry and pore topology. All Ga NMR spectra were acquired at a magnetic field of 21.1 T.

Sample		C_Q (^{71}Ga) (MHz)	C_Q (^{69}Ga) (MHz)	η_Q	Ω (ppm)	κ	α (˚)	β (˚)	γ (˚)
Experimental activated Ga-fumarate		19.4 (1)	30.9 (2)	0.13 (1)	160 (10)	0.6 (3)	0(10)	5 (3)	0(10)
Experimental Ga-fumarate-H_2O		24.6 (2)	39.7 (2)	0.09 (1)	250 (10)	1.0 (4)	0(10)	3 (3)	0(10)
Calculated activated Ga-fumarate[a,b]		19.2	30.7	0.15	157	0.41	234	87	182
Calculated Ga-fumarate-H_2O[a]		22.0	35.1	0.10	216	-0.07	91	85	3
Calculated Ga-fumarate-H_2O from a prior report[26] (space group: $P2_1/c$)[c]	**Ga1**	11.5	18.4	0.90	62	-0.25	204	42	174
	Ga2	11.5	18.4	0.91	62	-0.27	156	42	186
	Ga3	30.7	49.0	0.89	316	0.78	183	2	281
	Ga4	30.7	49.1	0.89	316	0.78	357	3	79
Experimental Ga-MIL-53[47]		19.1 (1)	30.2 (1)	0.06 (1)	80 (10)	1.0 (4)	0(10)	10 (4)	0(10)

[a] The calculated NMR parameters of activated Ga-fumarate and Ga-fumarate-H_2O are based on the crystal structure obtained after geometry optimization using the CASTEP software package, which employs plane-wave DFT methods and was also used to calculate all NMR parameters; see Experimental section for further details. [b] The crystal structure of activated Ga-fumarate was obtained by removing all water molecules from the channels of the Ga-fumarate-H_2O crystal structure. [C] The calculated NMR parameters of Ga-fumarate-H_2O are based on the crystal structure obtained after geometry optimization.

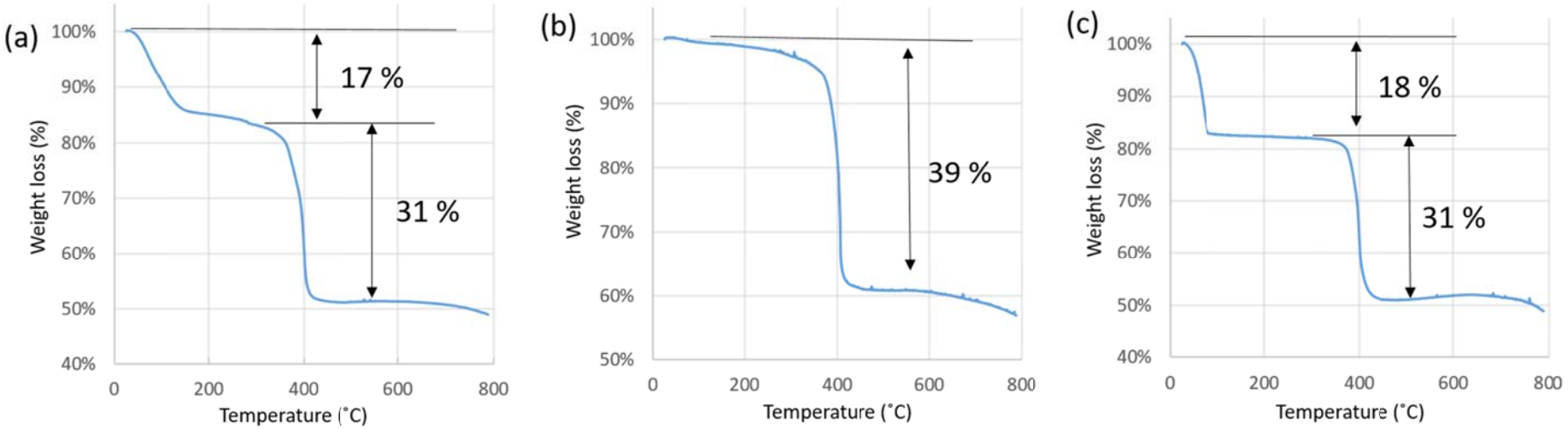

Figure S7. TGA plots of (a) In-fumarate-E(*as*) synthesized at 40 °C; (b) In-fumarate-E after activation under dynamic vacuum at 150 °C for 8 h; and (c) In-fumarate-E after activation followed by exposure to air (20 % r.h.) for 3 days to adsorb water (*i.e.*, In-fumarate-E-H_2O). Note the difference in y-axis scale between (b) and (a)/(c).

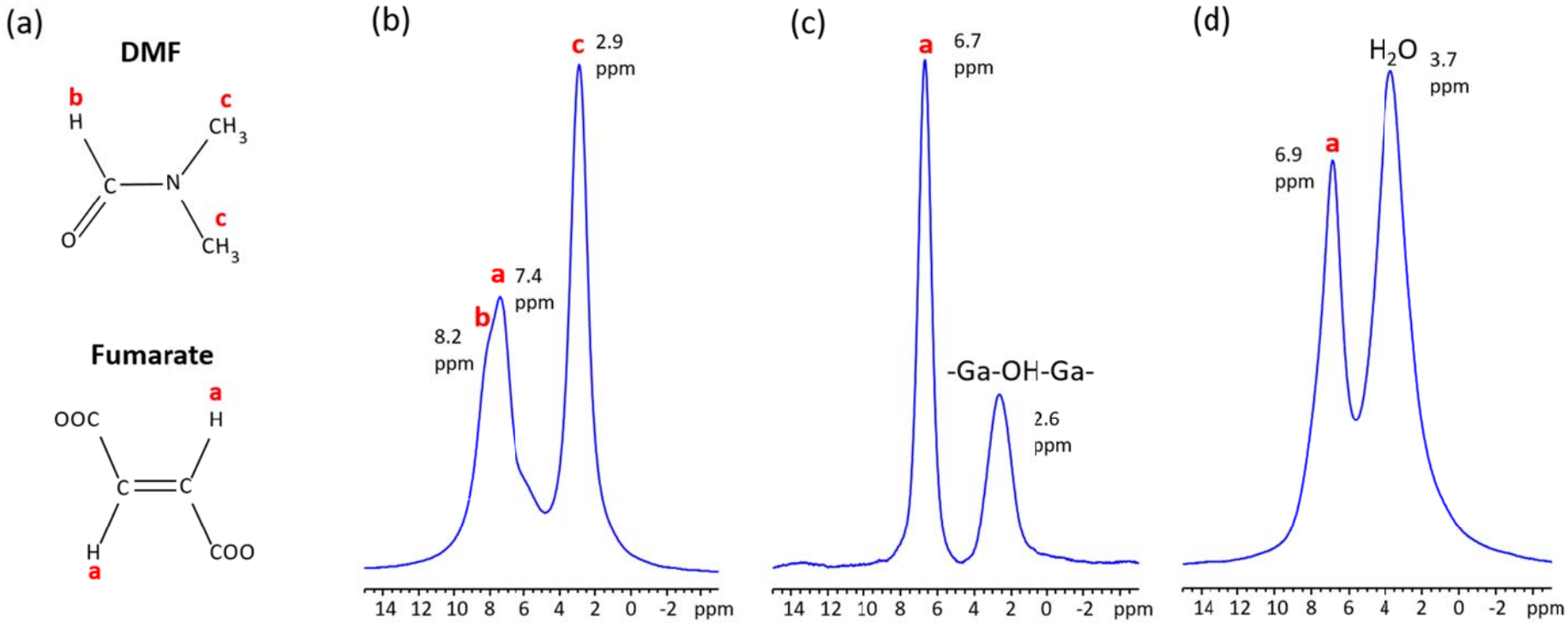

Figure S8. ^{1}H MAS NMR spectra of various forms of Ga-fumarate are pictured, as acquired at a magnetic field of 9.4 T and a spinning frequency of 14 kHz. The chemical structural formulas of the DMF guest and fumarate linker are illustrated in (a), with H atoms residing in distinct environments labeled with red lowercase letters. The ^{1}H NMR spectrum of as-made Ga-fumarate is shown in (b); the fumarate ^{1}H resonance is located at 7.4 ppm and the DMF ^{1}H resonances are found at 2.9 ppm and 8.2 ppm. The bridging –OH resonance in (b) is obscured by the more intense DMF ^{1}H resonance. In (c), the ^{1}H MAS NMR spectrum of activated Ga-fumarate is illustrated, where the fumarate linker ^{1}H resonance is now found at 6.7 ppm and the bridging –OH resonance can be resolved at 2.6 ppm due to the change in chemical environments after evacuating DMF. The ^{1}H MAS NMR spectrum of Ga-fumarate-H_2O is shown in (d), featuring a strong resonance at 3.7 ppm arising from adsorbed water, along with the fumarate resonance at 6.9 ppm. The bridging –OH resonance in (d) is concealed by the more intense –H_2O resonance.

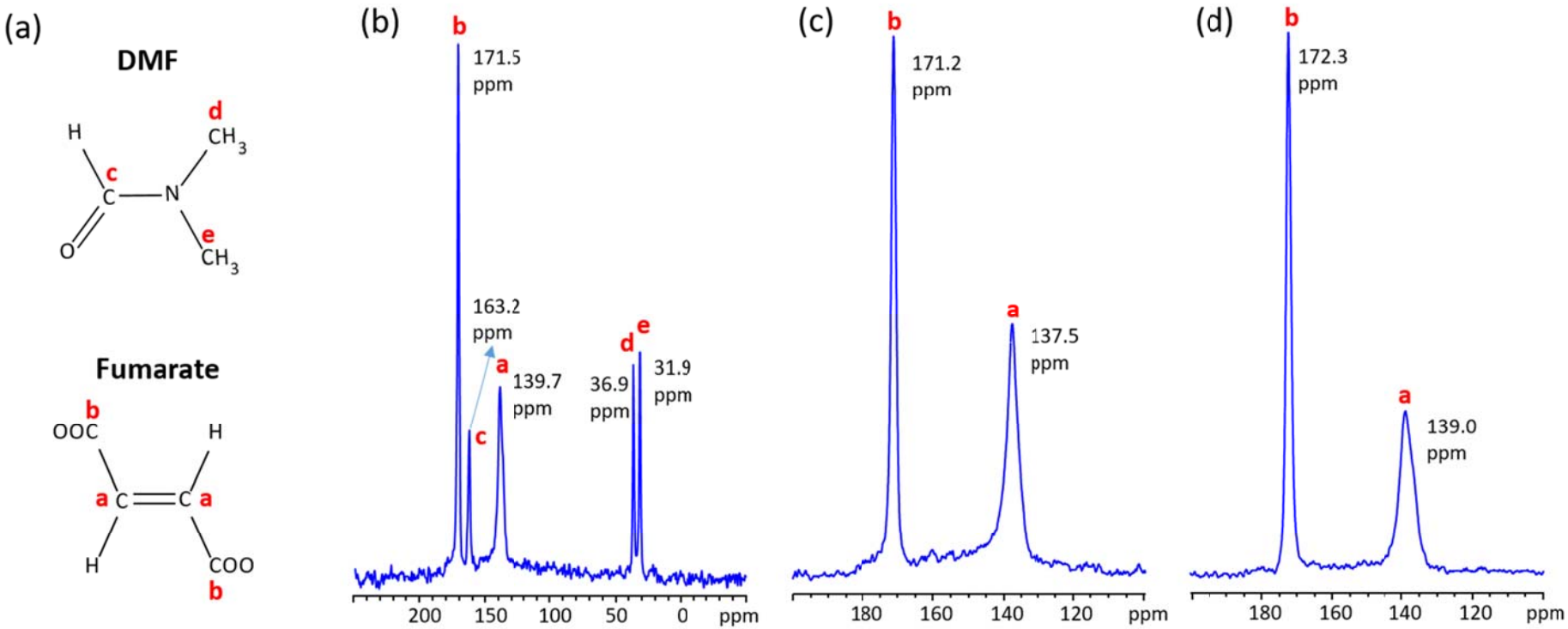

Figure S9. ^{13}C CP/MAS NMR spectra of various forms of Ga-fumarate are shown, as acquired at 9.4 T using a spinning frequency of 14 kHz. Panel (a) depicts the chemical structures of DMF guest molecules and the fumarate linker. Each type of C atom residing in a unique environment is labeled with a red letter. The ^{13}C CP/MAS NMR spectrum of as-made Ga-fumarate is shown in (b); the resonances at 163.2 ppm, 36.9 ppm and 31.9 ppm originate from DMF, while the resonances observed at 171.5 ppm and 139.7 ppm originate from the organic fumarate linkers. The ^{13}C CP/MAS NMR spectrum of activated Ga-fumarate is illustrated in (c), with the ^{13}C fumarate resonances located at 171.2 ppm and 137.5 ppm. Finally, the ^{13}C CP/MAS NMR spectrum of Ga-fumarate-H_2O is shown in (d), with the resonances from the organic fumarate linkers observed at 172.3 ppm and 139.0 ppm.

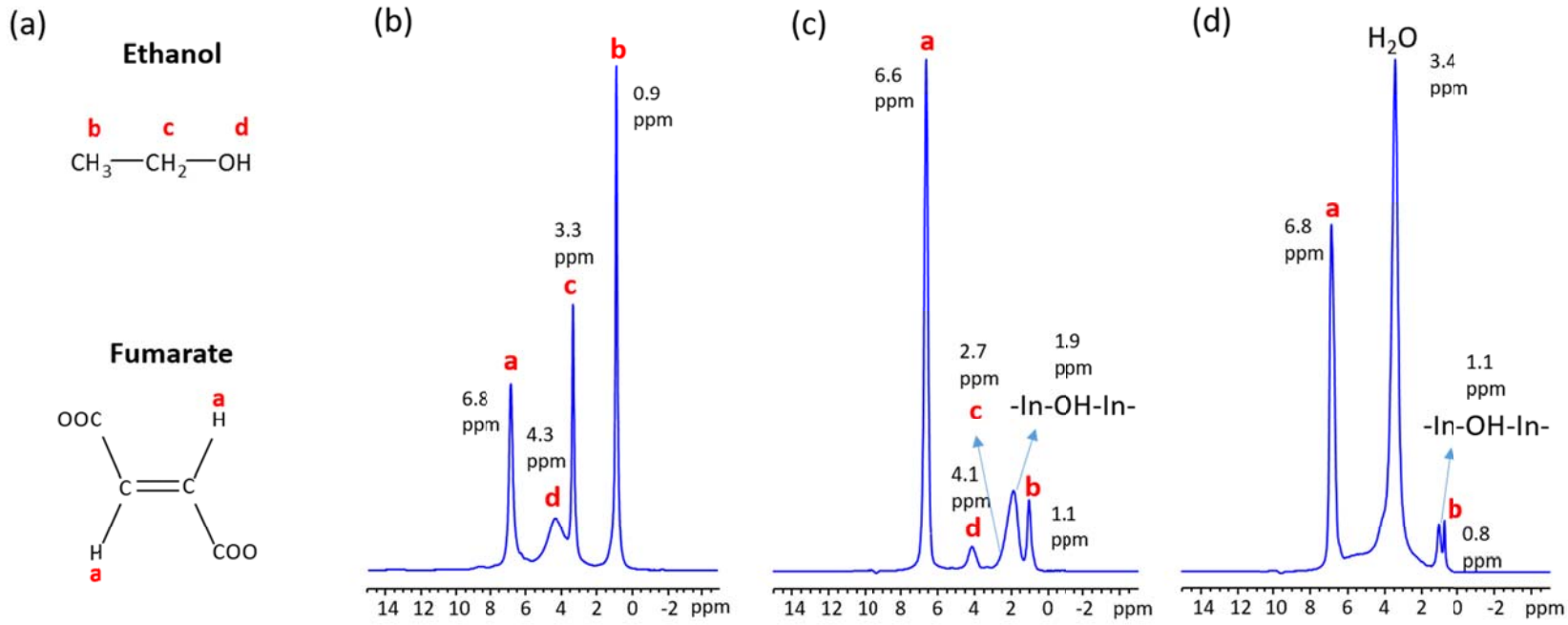

Figure S10. ^{1}H MAS NMR spectra of various forms of In-fumarate-E acquired at 21.1 T and a spinning frequency of 31.25 kHz. The chemical structural formulas of the ethanol guest and fumarate linker are illustrated in (a), with all unique H atoms labeled with red letters. It should be noted that the ^{1}H resonance from guest water molecules overlaps with the ^{1}H resonance of -OH groups in ethanol, giving rise to the broad resonance at 4.3 ppm in (b). The ^{1}H NMR spectrum of as-made In-fumarate-E is shown in (b); the fumarate ^{1}H resonance is located at 6.8 ppm and the ethanol ^{1}H resonances are found at 0.9 ppm, 3.3 ppm, and 4.3 ppm. In (c), the ^{1}H MAS NMR spectrum of activated In-fumarate-E is illustrated, where the fumarate linker ^{1}H resonance is now located at 6.6 ppm and the bridging –OH resonance is found at 1.9 ppm due to changes in the hydrogen local environment after removing guest ethanol molecules. The ethanol ^{1}H resonances in activated In-fumarate-E also indicate that it is difficult to fully remove all guest ethanol molecules from this MOF. The ^{1}H MAS NMR spectrum of In-fumarate-E-H_2O is shown in (d), featuring a large resonance at 3.4 ppm arising from adsorbed water, along with the fumarate resonance at 6.8 ppm. The bridging –OH resonance in (d) is observed at 1.1 ppm rather than 1.9 ppm due to the change in local chemical environments after water adsorption.

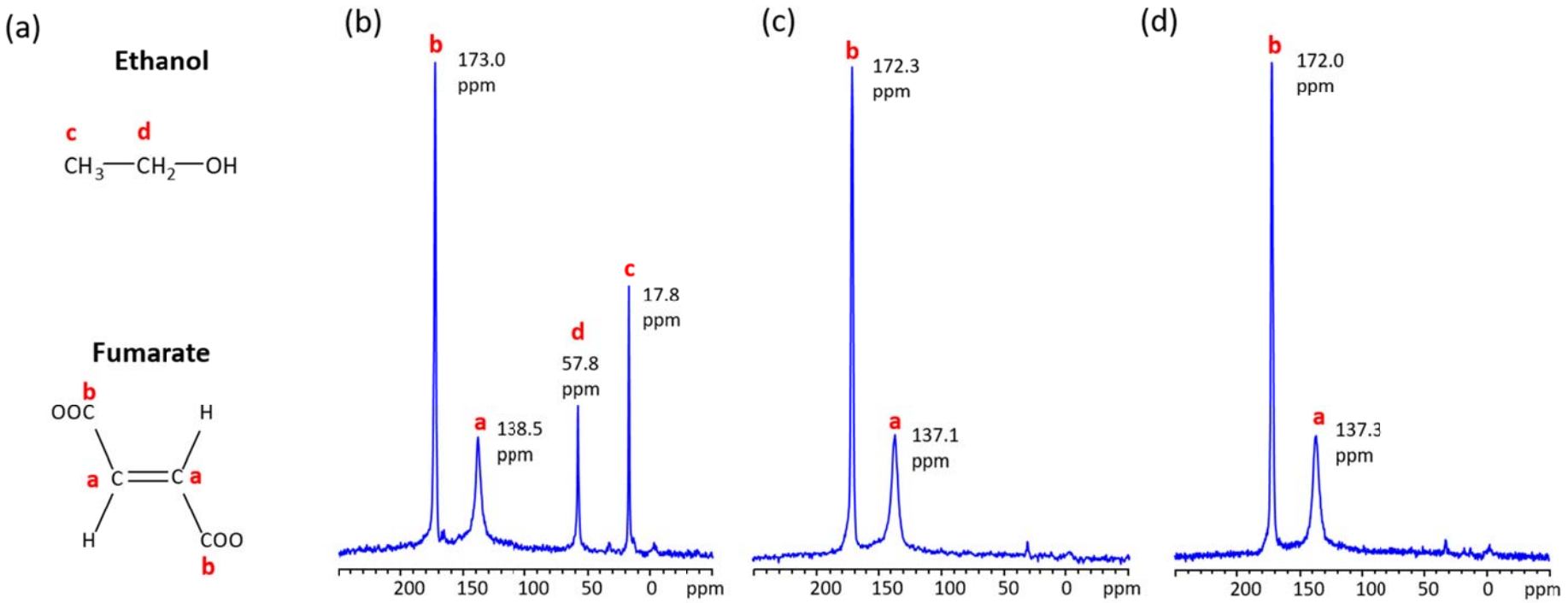

Figure S11. ^{13}C CP/MAS NMR spectra of various forms of In-fumarate-E are shown, as acquired at 9.4 T using a spinning frequency of 14 kHz. Panel (a) depicts the chemical structures of ethanol guest molecules and the fumarate linker. Each type of C atom residing in a unique environment is labeled with a red letter. The ^{13}C CP/MAS NMR spectrum of as-made In-fumarate-E is shown in (b); the resonances at 17.8 ppm and 57.8 ppm originate from ethanol, while the resonances observed at 173.0 ppm and 138.5 ppm correspond to carbon on the organic fumarate linkers. The ^{13}C CP/MAS NMR spectrum of activated In-fumarate-E is illustrated in (c), with the ^{13}C fumarate resonances located at 172.3 ppm and 137.1 ppm. Finally, the ^{13}C CP/MAS NMR spectrum of In-fumarate-E-H_2O is shown in (d), with the resonances from the organic fumarate linkers observed at 172.0 ppm and 137.3 ppm.

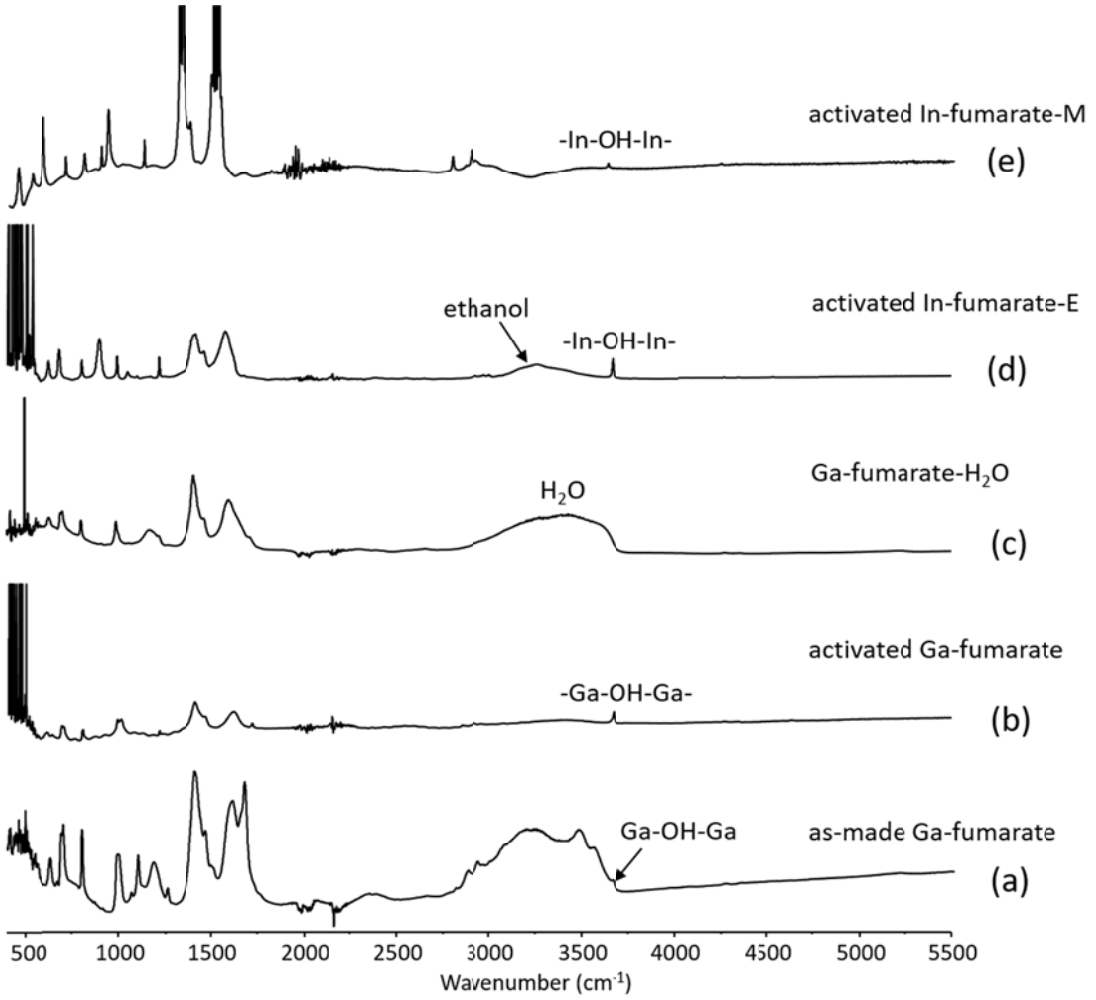

Figure S12. The IR spectra of various forms of fumarate MOFs are shown. The as-made Ga-fumarate IR spectrum is shown in (a). The broad adsorption in (a) from 2800-3700 cm^{-1} arises from water; the small secondary features on this broad peak are caused by C-H vibrations in the trapped residual solvent (DMF), while O-H stretch of bridging hydroxyl groups gives rise to the minor feature at 3657 cm^{-1}. In (b), the IR spectrum of activated Ga-fumarate is shown, which lacks the broad adsorption from 2800-3700 cm^{-1} due to the removal of guest H_2O molecules and residual solvent from the MOF channels. It is important to note that the O-H vibration of bridging hydroxyl groups persists at 3670 cm^{-1} and is especially visible in the activated sample. The IR spectrum in (c) corresponds to hydrated Ga-fumarate-H_2O, and the broad adsorption ranging from 2700 to 3700 cm^{-1} is again visible due to the presence of adsorbed water in the MOF channels. The IR spectrum of activated In-fumarate-E is shown in (d); the O-H vibration of bridging hydroxyl groups gives rise to the small feature at 3666 cm^{-1}, while the broad adsorption from 3050 to 3570 cm^{-1} arises from residual ethanol not removed by the activation process. The activated In-fumarate-M IR spectrum is illustrated in (e), and it is apparent the O-H vibration of bridging hydroxyl groups at 3666 cm^{-1} is much less intense than in previous IR spectra, suggesting there are fewer bridging –OH groups, which we hypothesize is due to replacement with bridging $–OCH_3$ groups.

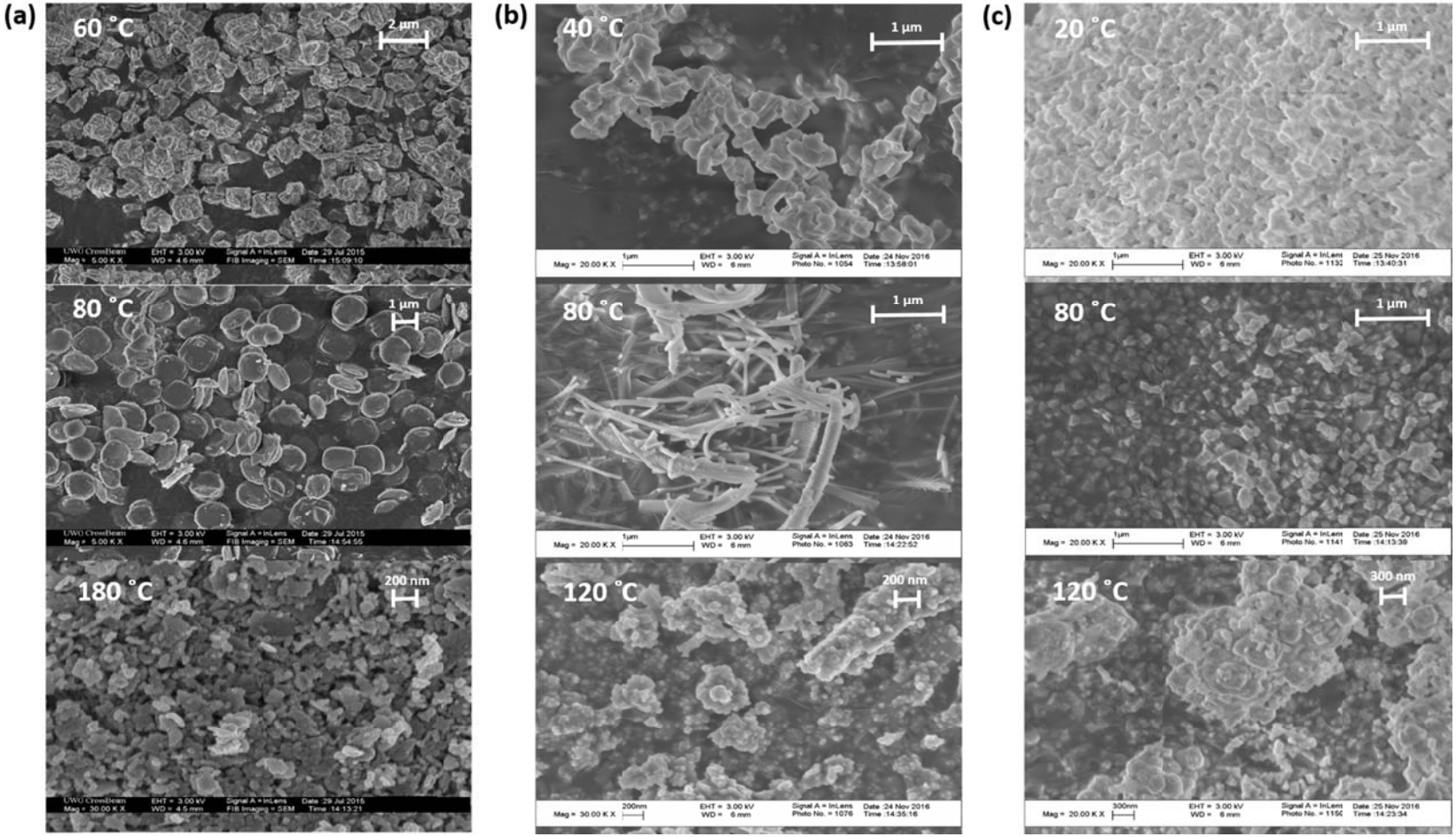

Figure S13. The SEM images of as-made (a) Ga-fumarate, (b) In-fumarate-E, and (c) In-fumarate-M samples synthesized at various temperatures are illustrated. From this data, it is evident that each synthetic temperature yields a product of a different morphology.

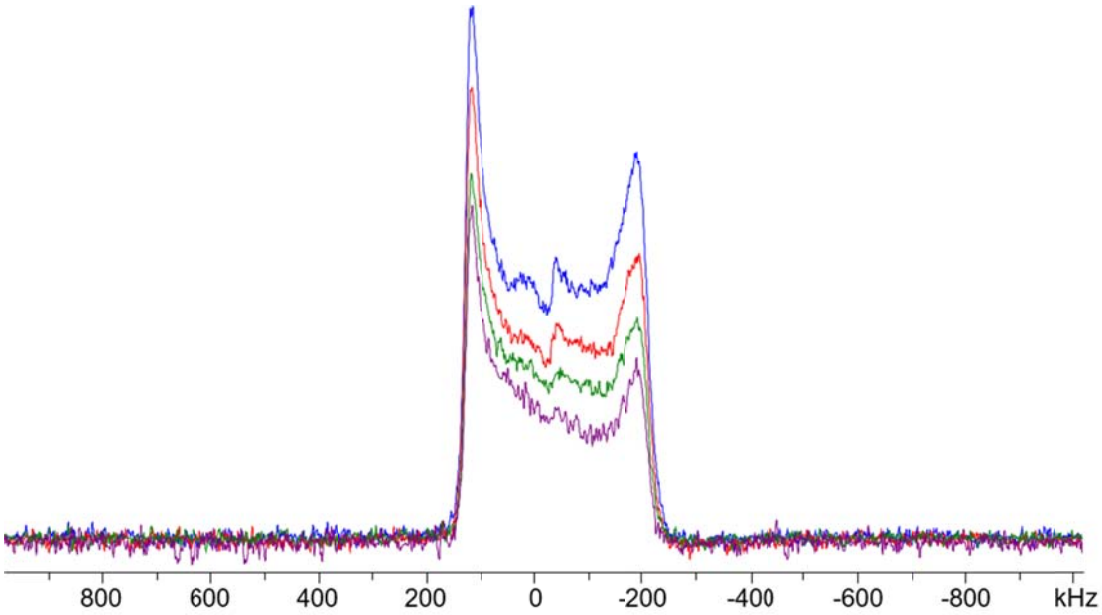

Figure S14. An illustration of ^{71}Ga T_2 relaxation anisotropy in the static ^{71}Ga NMR spectrum of Ga-fumarate-H_2O at 21.1 T. Using a standard quadrupolar echo pulse sequence of the form ($\pi/2$-τ_1-$\pi/2$-τ_2-acq), these spectra were acquired using τ_1 echo values of 10 µs (blue trace), 70 µs (red), 120 µs (green) and 200 µs (purple). Note the pronounced reduced intensity of the low-frequency discontinuity or "horn" and concomitant departure from an idealized quadrupolar powder pattern shape when longer τ_1 values are employed, which clearly indicates that T_2 relaxation anisotropy is present.

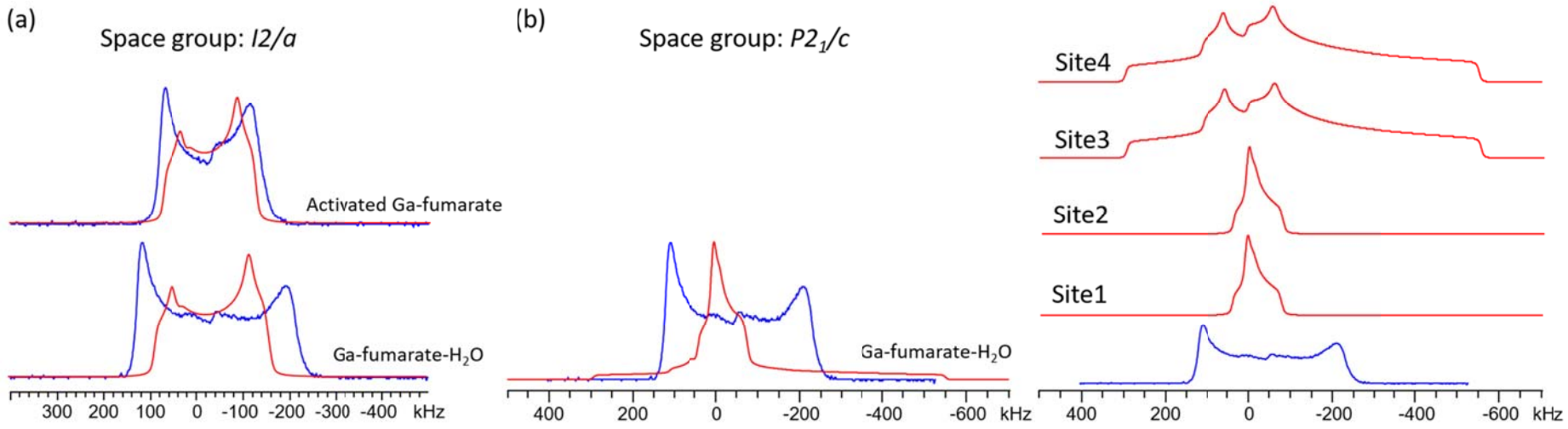

Figure S15. A comparison of experimental (blue) and plane-wave DFT calculated (red) static ^{71}Ga NMR spectra at 21.1 T are shown. In (a), the calculated spectra are obtained from our refined Ga-fumarate-H_2O structure with a space group of *I2/a*, while in (b), the overall calculated spectrum is generated from the previously reported Ga-fumarate-H_2O structure with a space group of $P2_1/c$. The calculated ^{71}Ga NMR spectra at 21.1 T of all four distinct Ga sites (red) along with the experimental spectrum (blue) are shown on the right side of (b). Note the fair agreement between experimental and calculated spectra in (a), while the calculated and experimental spectra are quite dissimilar in (b).

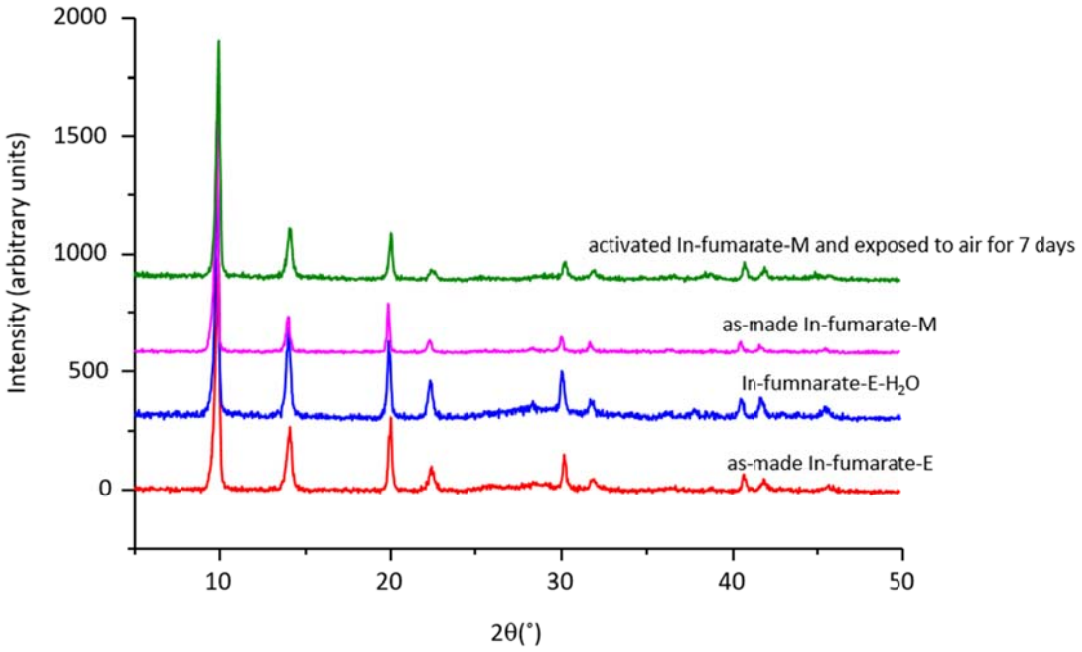

Figure S16. A comparison of the pXRD patterns obtained from various forms of the In-fumarate-E and In-fumarate-M MOFs.

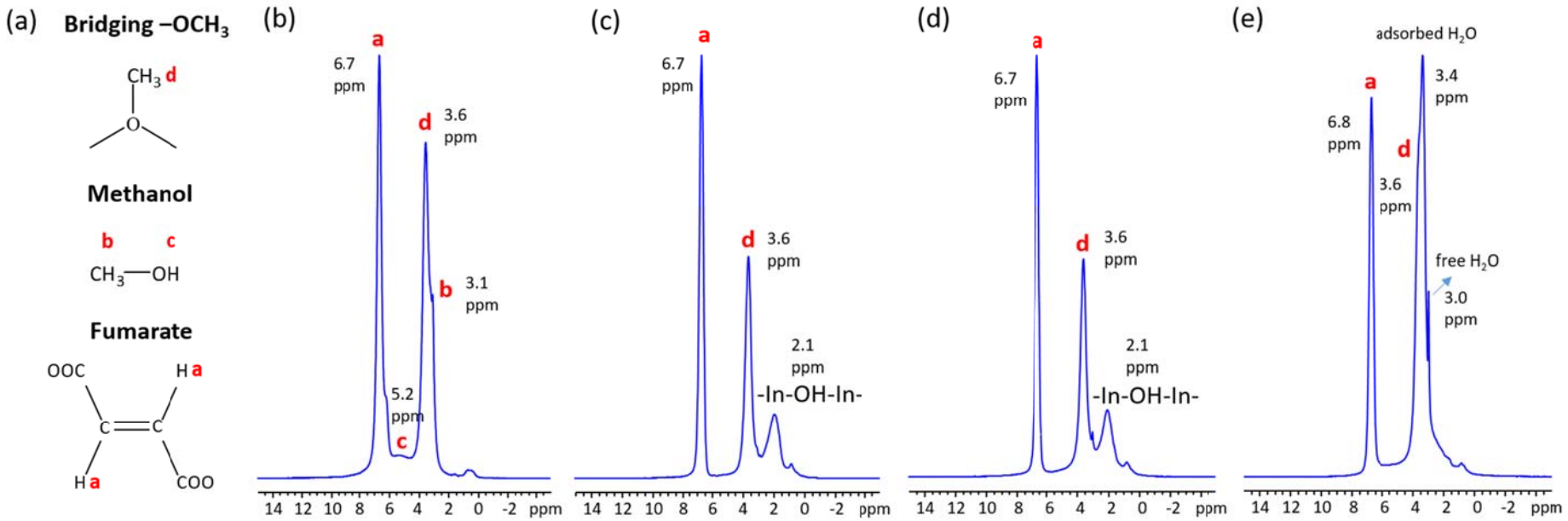

Figure S17. ^{1}H MAS NMR spectra of various forms of In-fumarate-M are pictured, as acquired at 21.1 T and a spinning frequency of 31.25 kHz. The chemical structures of the bridging –OCH_3 group, methanol guest, and fumarate linker are illustrated in (a), with H atoms residing in distinct environments labeled with red letters. The ^{1}H NMR spectrum of as-made In-fumarate-M is given in (b); the fumarate ^{1}H resonance is located at 6.7 ppm and the methanol ^{1}H resonances are found at 3.6 ppm and 5.2 ppm. In (c), the ^{1}H MAS NMR spectrum of activated In-fumarate-M is shown, where the fumarate linker ^{1}H resonance is at 6.7 ppm and the bridging –OH resonance is found at 2.1 ppm. The ^{1}H resonance of bridging –OCH_3 is located at 3.6 ppm. The ^{1}H MAS NMR spectrum of activated In-fumarate-M followed by exposure to air (20 % r.h.) for 7 days is shown in (d) and appears similar to that of activated In-fumarate-M, indicating that very little or no water had been adsorbed inside the MOF. In (e), the ^{1}H MAS NMR spectrum of activated In-fumarate-M followed by exposure to 80 % r.h. air for 2 hours is shown, where the ^{1}H resonance of adsorbed water is clearly visible at 3.4 ppm. The ^{1}H MAS NMR spectra indicate enhanced hydrophobicity of the In-fumarate-M MOF at low humidity.

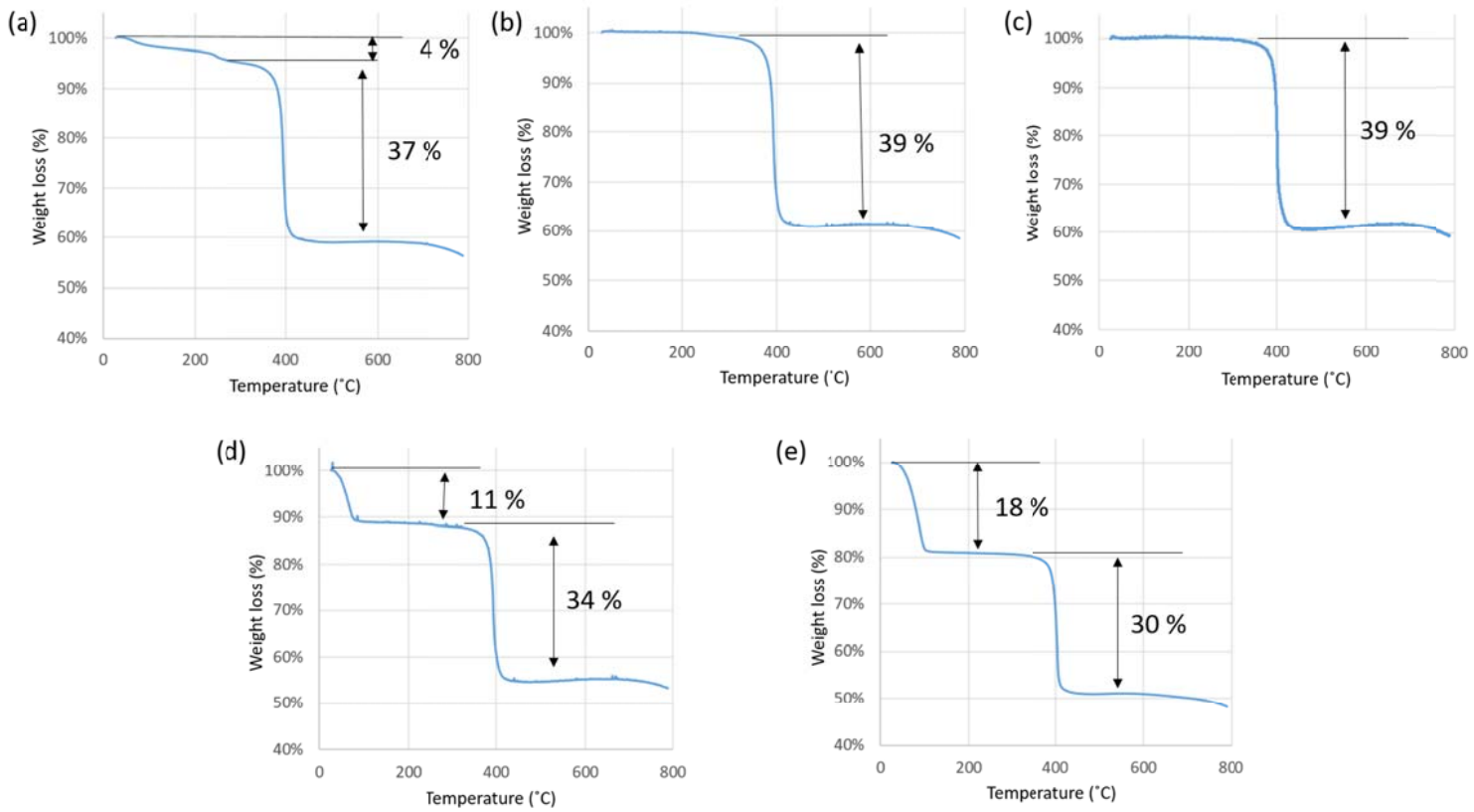

Figure S18. TGA plots of (a) In-fumarate-M(*as*) synthesized at 20 °C; (b) In-fumarate-M after activation under dynamic vacuum at 150 °C for 8 h; (c) In-fumarate-M after activation followed by exposure to air (20 % r.h.) for 7 days; (d) In-fumarate-M(*as*) after activation followed by exposure to 80 % r.h. for 2 hours; (e) In-fumarate-M after activation followed by exposure to 80 % r.h. for 24 hours. The calculated chemical formula of In-fumarate-M(*as*) based on TGA is $In(OH)_{0.2}(OCH_3)_{0.8}(C_4H_2O_4)\cdot 0.33CH_3OH$, with a carbon percentage of 22.99 % and H percentage of 2.21 %, which is comparable to the elemental analysis results (C: 21.75 %, H: 1.70 %, N: 0.54 %).

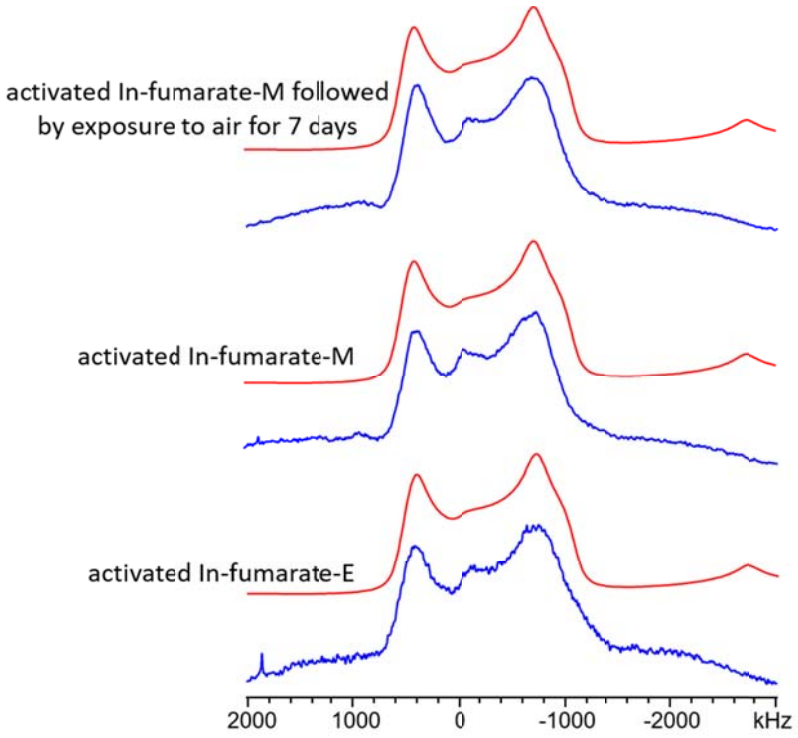

Figure S19. Static ^{115}In NMR spectra of various form of In-fumarate MOFs acquired at 21.1 T. All versions of the In-fumarate MOF give rise to similar ^{115}In NMR spectra, revealing that the In metal centers within these three MOFs reside in similar local environments. The residual intensity outside the main powder pattern arises from the ^{115}In satellite transitions.

Table S2. Experimentally determined ^{115}In NMR parameters of activated In-fumarate-E, In-fumarate-E-H_2O, activated In-fumarate-M, and activated In-fumarate-M followed by exposure to air (20 % r.h.) for 7 days. All experimental static ^{115}In NMR spectra were acquired at a magnetic field of 21.1 T. Note that in all instances, the ^{115}In CS parameters (δ_{iso}, Ω, and κ) did not have a significant impact and were all determined to be zero.

Sample	C_Q (^{115}In) (MHz)	η_Q
Activated In-fumarate-M	188 (2)	0.20 (2)
Activated In-fumarate-M after exposure to air (20 % r.h.) for 7 days	189 (3)	0.20 (2)
Activated In-fumarate-E	192 (2)	0.21 (2)
Experimental In-fumarate-E-H_2O	260 (3)	0.00 (2)

Table S3. The measured BET surface areas (in units of m^2/g) of Ga-fumarate samples synthesized at different temperatures using different molar ratios of $Ga(NO_3)_3$ and fumaric acid. The $Ga(NO_3)_3$: fumaric acid ratio is denoted as Ga: FA in the table.

Temperature (˚C)		**60**	**80**	**100**	**120**	**140**	**160**	**180**
Ga: FA	**1：1**	723	851	790	715	716	525	159
	1：2	748	833	720	696	666	481	116

Table S4. The measured BET surface areas (in units of m^2/g) of In-fumarate-E and In-fumarate-M samples synthesized at different temperatures using different molar ratios of $In(NO_3)_3$ and fumaric acid. The $In(NO_3)_3$: fumaric acid ratio is denoted as In: FA in the table.

Temperature (˚C)			**20**	**40**	**60**	**80**	**100**	**120**
In-fumarate-E	**In : FA**	1 : 1	596	695	691	503	490	383
		1 : 2	632	708	692	595	515	410
In-fumarate-M	**In : FA**	1 : 1	599	478	464	332	340	317
		1 : 2	237	478	551	385	373	351

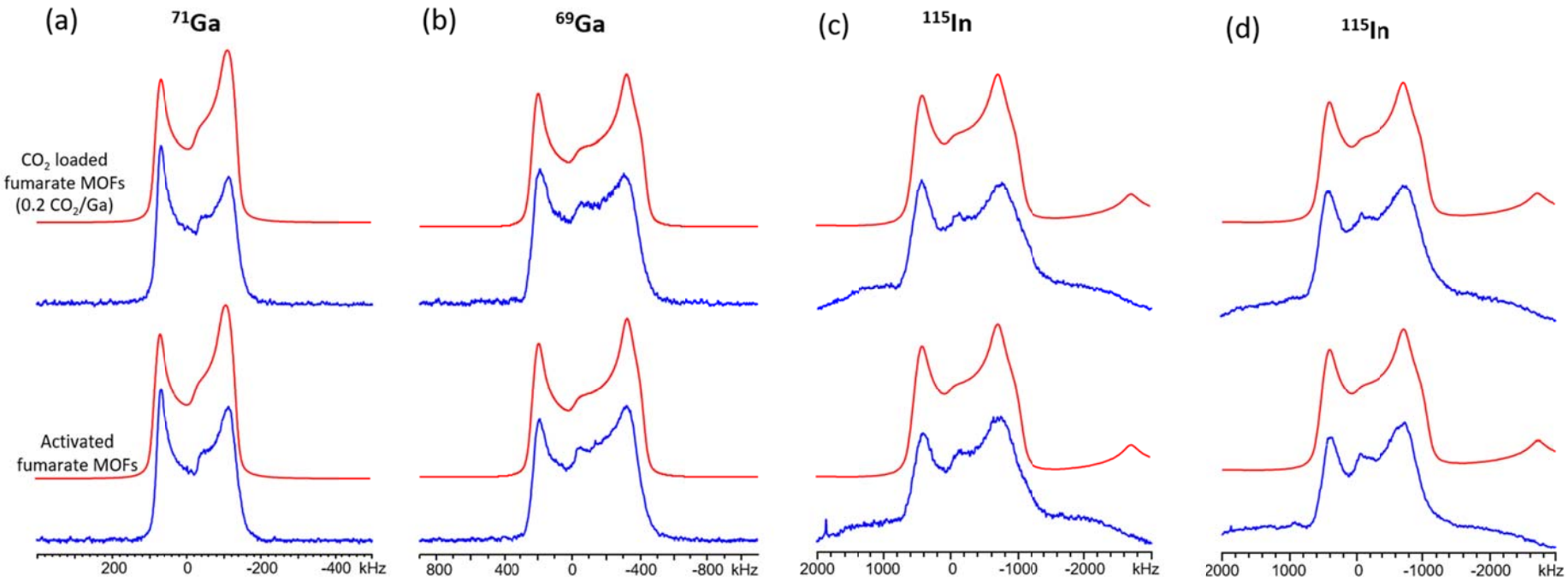

Figure S20. The static ^{71}Ga and ^{69}Ga NMR spectra of activated and CO_2-loaded Ga-fumarate are shown in (a) and (b), respectively, along with the ^{115}In NMR spectra of (c) activated and (d) CO_2 loaded In-fumarate-E and In-fumarate-M. All ^{69}Ga, ^{71}Ga, and ^{115}In spectra were acquired at 21.1 T. The activated and CO_2-loaded spectra and associated NMR parameters (Table S5 and Table S6) are similar, indicating that the local environments about the Ga and In centers are generally unaffected by CO_2 adsorption within these MOFs. The residual intensity outside the main powder pattern in (c) and (d) arises from the ^{115}In satellite transitions.

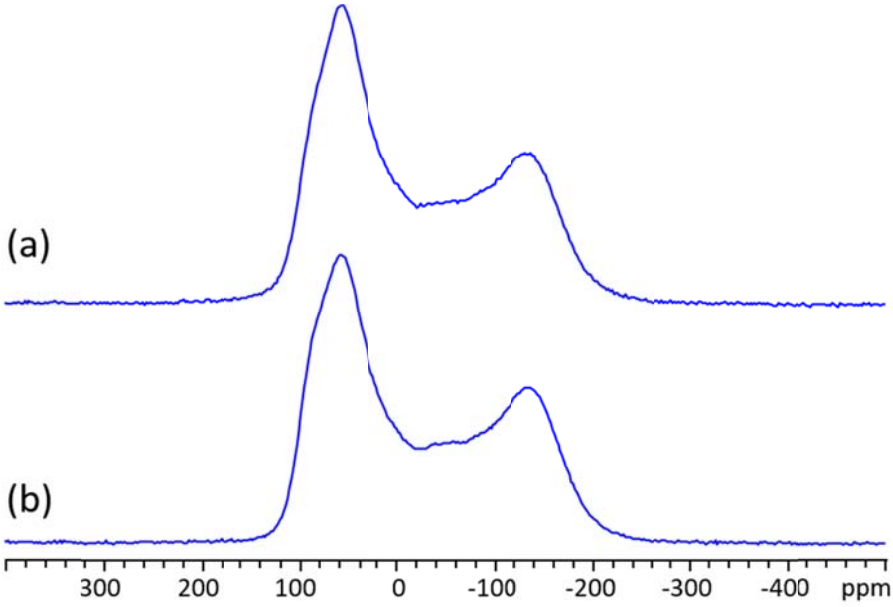

Figure S21. The static ^{27}Al NMR spectrum of activated Al-fumarate is shown in (a). For comparison, the static ^{27}Al NMR spectrum of CO_2-loaded Al-fumarate (loading level: 0.2 CO_2/Al) is depicted in (b). Note the lack of significant differences between these spectra, suggesting that CO_2 and aluminum do not engage in any significant interaction within Al-fumarate, and the Al local environment is not significantly influenced or perturbed by CO_2 adsorption. Both spectra were acquired at a magnetic field of 9.4 T.

Table S5. A comparison of the experimental ^{69}Ga and ^{71}Ga NMR parameters of activated and CO_2 loaded Ga-fumarate. In all instances, δ_{iso} = 0 ppm.

Sample	C_Q (^{71}Ga) (MHz)	C_Q(^{69}Ga) (MHz)	η_Q	Ω (ppm)	κ
Activated Ga-fumarate	19.4 (1)	30.9 (2)	0.13 (1)	160 (10)	0.6 (3)
CO_2 loaded Ga-fumarate	19.4 (1)	30.9 (2)	0.14 (1)	160 (10)	0.6 (4)

Table S6. A comparison of the experimental ^{115}In NMR parameters of activated and CO_2 loaded In-fumarate-E and In-fumarate-M.[a]

Sample	C_Q (^{115}In) (MHz)	η_Q
Activated In-fumarate-E	192 (2)	0.21 (2)
CO_2 loaded In-fumarate-E	192 (3)	0.21 (2)
Activated In-fumarate-M	188 (2)	0.20 (2)
CO_2 loaded In-fumarate-M	188 (2)	0.20 (2)

[a] CS parameters do not influence the ^{115}In powder patterns due to the extreme dominance of the EFG tensor on spectral appearance. Simulations employed δ_{iso} = 0 ppm, Ω = 0 ppm, and κ = 0.

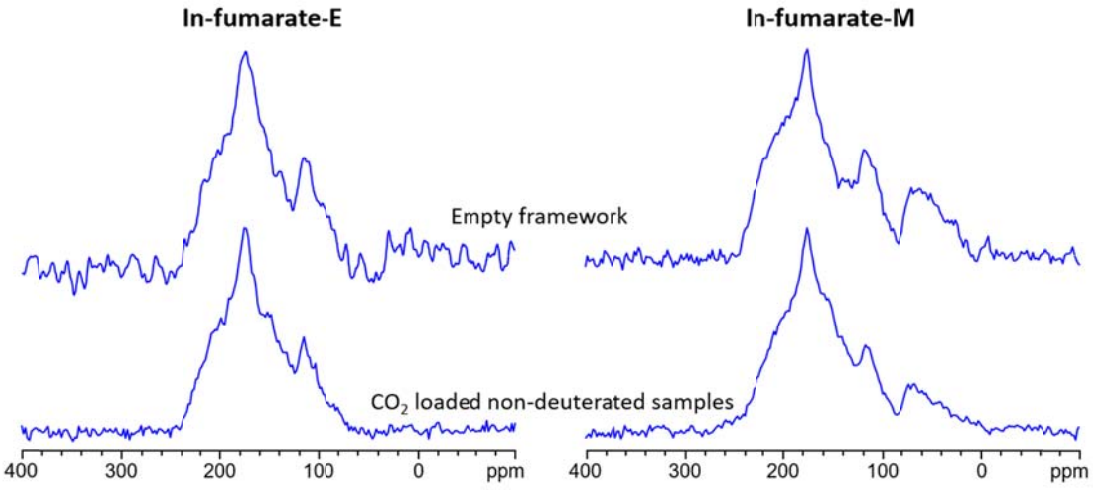

Figure S22. Static ^{13}C CP NMR spectra of activated and CO_2-loaded In-fumarate-E and In-fumarate-M MOFs at a temperature of 133 K and field of 9.4 T are shown. Due to a relatively weak CO_2 binding strength and a correspondingly long H-CO_2 distance, an adsorbed CO_2 resonance cannot be detected in CO_2 loaded non-deuterated samples.

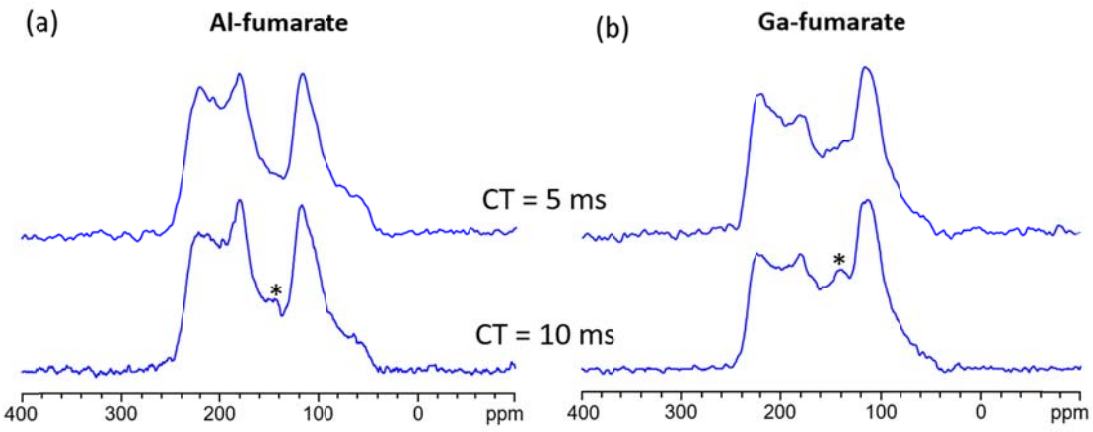

Figure S23. Static ^{13}C CP NMR spectra of the CO_2-loaded (a) Al-fumarate and (b) Ga-fumarate MOFs using different contact times (CTs) at a temperature of 133 K and field of 9.4 T are shown. For both MOFs, the CO_2 resonance (denoted * in the figure) was only observed when a long 10 ms CT was employed.

Table S7. The observed, or apparent, ^{13}C CS parameters of CO_2 adsorbed within Al-fumarate, Ga-fumarate, In-fumarate-E and In-fumarate-M as obtained from analytical simulations of static ^{13}C DEPTH-echo VT NMR spectra. A well-defined ^{13}C powder pattern within CO_2-loaded Ga-fumarate can be observed from 173 K to 133 K, while a well-defined ^{13}C powder pattern can be observed in CO_2-loaded In-fumarate-E and In-fumarate-M from 153 K to 133 K.

T	Al-fumarate			Ga-fumarate			In-fumarate-E			In-fumarate-M		
	δ_{iso} (ppm)	Ω (ppm)	κ	δ_{iso} (ppm)	Ω (ppm)	κ	δ_{iso} (ppm)	Ω (ppm)	κ	δ_{iso} (ppm)	Ω (ppm)	κ
373 K	125(1)	26(1)	1.00(2)									
353 K	125(1)	26(1)	1.00(2)									
333 K	125(1)	26(1)	1.00(2)									
313 K	126(1)	27(1)	1.00(2)									
293 K	126(1)	27(1)	1.00(2)									
273 K	126(1)	28(1)	1.00(2)									
253 K	126(1)	28(1)	1.00(2)									
233 K	126(1)	30(1)	1.00(2)									
213 K	125(1)	35(1)	1.00(2)									
193 K	125(1)	36(1)	1.00(2)									
173 K	125(1)	45(1)	1.00(2)	126(1)	40(1)	0.50(2)						
153 K	125(1)	54(1)	1.00(2)	126(1)	56(1)	0.76(2)	126(2)	58(1)	1.00(2)	125(2)	60(1)	1.00(2)
133 K	125(1)	62(1)	1.00(2)	126(1)	68(1)	0.88(2)	127(2)	85(2)	1.00(2)	128(2)	95(2)	1.00(2)

References

(1) Toby, B. H.; Von Dreele, R. B. GSAS-II: The Genesis of a Modern Open-Source All Purpose Crystallography Software Package. *J. Appl. Cryst.* **2013**, *46*, 544-549.
(2) Rietveld, H. M. Line Profiles of Neutron Powder-Diffraction Peaks for Structure Refinement. *Acta Cryst.* **1967**, *22*, 151-152.
(3) Coelho, A. A. *Topas - Academic*, v. 6.0; Coelho Software: Brisbane, Australia, 2016.
(4) Hayashi, S.; Hayamizu, K. Chemical Shift Standards in High-Resolution Solid-State NMR (1) ^{13}C, ^{29}Si, and ^{1}H Nuclei. *Bull. Chem. Soc. Jpn.* **1991**, *64*, 685-687.
(5) Dybowski, C.; Neue, G. Solid State ^{207}Pb NMR Spectroscopy. *Prog. Nucl. Magn. Reson. Spectrosc.* **2002**, *41*, 153-170.
(6) Zhang, Y.; Lucier, B. E. G.; Huang, Y. Deducing CO_2 Motion, Adsorption Locations and Binding Strengths in a Flexible Metal-Organic Framework without Open Metal Sites. *Phys. Chem. Chem. Phys.* **2016**, *18*, 8327-8341.
(7) Fulmer, G. R.; Miller, A. J. M.; Sherden, N. H.; Gottlieb, H. E.; Nudelman, A.; Stoltz, B. M.; Bercaw, J. E.; Goldberg, K. I. NMR Chemical Shifts of Trace Impurities: Common Laboratory Solvents, Organics, and Gases in Deuterated Solvents Relevant to the Organometallic Chemist. *Organometallics* **2010**, *29*, 2176-2179.
(8) Harris, R. K.; Becker, E. D.; de Menezes, S. M. C.; Goodfellow, R.; Granger, P. NMR Nomenclature: Nuclear Spin Properties and Conventions for Chemical Shifts - IUPAC Recommendations 2001. *Pure Appl. Chem*, **2001**, *73*, 1795-1818.
(9) Massiot, D.; Farnan, I.; Gautier, N.; Trumeau, D.; Florian, P.; Grandinetti, P. J. $^{69,71}Ga$ Solid-State Static, MAS and DAS NMR-Study of β-Ga_2O_3. *J. Chim. Phys.* **1995**, *92*, 1847-1850.
(10) Bonhomme, C.; Gervais, C.; Babonneau, F.; Coelho, C.; Pourpoint, F.; Azaïs, T.; Ashbrook, S. E.; Griffin, J. M.; Yates, J. R.; Mauri, F.; Pickard, C. J. First-Principles Calculation of NMR Parameters Using the Gauge Including Projector Augmented Wave Method: A Chemist's Point of View. *Chem. Rev.* **2012**, *112*, 5733-5779.
(11) Clark, S. J.; Segall, M. D.; Pickard, C. J.; Hasnip, P. J.; Probert, M. J.; Refson, K.; Payne, M. C. First Principles Methods Using CASTEP. *Z. Kristall.* **2005**, *220*, 567-570.
(12) Segall, M. D.; Lindan, P. J. D.; Probert, M. J.; Pickard, C. J.; Hasnip, P. J.; Clark, S. J.; Payne, M. C. First-Principles Simulation: Ideas, Illustrations and the CASTEP Code. *J. Phys. Condens. Matter* **2002**, *14*, 2717-2744.
(13) Perdew, J. P.; Burke, K.; Ernzerhof, M. Generalized Gradient Approximation Made Simple. *Phys. Rev. Lett.* **1996**, *77*, 3865-3868.
(14) Grimme, S. Semiempirical GGA‐Type Density Functional Constructed with a Long‐Range Dispersion Correction. *J. Comput. Chem.* **2006**, *27*, 1787-1799.
(15) Yates, J. R.; Pickard, C. J.; Mauri, F. Calculation of NMR Chemical Shifts for Extended Systems Using Ultrasoft Pseudopotentials. *Phys. Rev. B* **2007**, *76*, 024401(1) - 024401(11).
(16) Pickard, C. J.; Mauri, F. All-Electron Magnetic Response with Pseudopotentials: NMR Chemical Shifts. *Phys. Rev. B* **2001**, *63*, 245101(1) - 245101(13).
(17) K. Eichele, R. E. W., *WSolids1: Solid-State NMR Spectrum Simulation*. v 1.20.21. University of Tübingen: Tübingen, Germany, 2013.

(18) Perras, F. A.; Widdifield, C. M.; Bryce, D. L. QUEST—Quadrupolar Exact Software: A Fast Graphical Program for the Exact Simulation of NMR and NQR Spectra for Quadrupolar Nuclei. *Solid State Nucl. Magn. Reson.* **2012**, *45–46*, 36-44.
(19) Vold, R. L.; Hoatson, G. L. Effects of Jump Dynamics on Solid State Nuclear Magnetic Resonance Line Shapes and Spin Relaxation Times. *J. Magn. Reson.* **2009**, *198*, 57-72.
(20) Rose, M. E., *Elementary Theory of Angular Momentum*. Wiley: New York, 1957.
(21) Alvarez, E.; Guillou, N.; Martineau, C.; Bueken, B.; Van de Voorde, B.; Le Guillouzer, C.; Fabry, P.; Nouar, F.; Taulelle, F.; de Vos, D.; Chang, J.-S.; Cho, K. H.; Ramsahye, N.; Devic, T.; Daturi, M.; Maurin, G.; Serre, C. The Structure of the Aluminum Fumarate Metal–Organic Framework A520. *Angew. Chem. Int. Ed.* **2015**, *54*, 3664-3668.